RESEARCH ARTICLE

Force-dependent focal adhesion assembly and disassembly: A computational study

Kailas Shankar Honasoge[1‡], **Zeynep Karagöz**[1‡], **Benjamin T. Goult**[2], **Haguy Wolfenson**[3], **Vanessa L. S. LaPointe**[1], **Aurélie Carlier**[1]*

1 Department of Cell Biology–Inspired Tissue Engineering, MERLN Institute for Technology-Inspired Regenerative Medicine, Maastricht University, Maastricht, the Netherlands, **2** School of Biosciences, University of Kent, Canterbury, United Kingdom, **3** Department of Genetics and Developmental Biology, Rappaport Faculty of Medicine, Technion – Israel Institute of Technology, Haifa, Israel

‡These authors share first authorship on this work.
* a.carlier@maastrichtuniversity.nl

Abstract

Cells interact with the extracellular matrix (ECM) via cell–ECM adhesions. These physical interactions are transduced into biochemical signals inside the cell which influence cell behaviour. Although cell–ECM interactions have been studied extensively, it is not completely understood how immature (nascent) adhesions develop into mature (focal) adhesions and how mechanical forces influence this process. Given the small size, dynamic nature and short lifetimes of nascent adhesions, studying them using conventional microscopic and experimental techniques is challenging. Computational modelling provides a valuable resource for simulating and exploring various "what if?" scenarios in silico and identifying key molecular components and mechanisms for further investigation. Here, we present a simplified mechano-chemical model based on ordinary differential equations with three major proteins involved in adhesions: integrins, talin and vinculin. Additionally, we incorporate a hypothetical signal molecule that influences adhesion (dis)assembly rates. We find that assembly and disassembly rates need to vary dynamically to limit maturation of nascent adhesions. The model predicts biphasic variation of actin retrograde velocity and maturation fraction with substrate stiffness, with maturation fractions between 18–35%, optimal stiffness of ∼ 1 pN/nm, and a mechanosensitive range of 1-100 pN/nm, all corresponding to key experimental findings. Sensitivity analyses show robustness of outcomes to small changes in parameter values, allowing model tuning to reflect specific cell types and signaling cascades. The model proposes that signal-dependent disassembly rate variations play an underappreciated role in maturation fraction regulation, which should be investigated further. We also provide predictions on the changes in traction force generation under increased/decreased vinculin concentrations, complementing previous vinculin overexpression/knockout experiments in different cell types. In summary, this work proposes a model framework to robustly simulate the mechanochemical processes underlying adhesion maturation and maintenance, thereby enhancing our fundamental knowledge of cell–ECM interactions.

Author summary

The immediate environment of a cell is vastly different in healthy and diseased tissue and influences numerous intracellular processes. Mechanical and chemical properties of the extracellular matrix (ECM) impact cellular processes through various pathways, enabling cells to 'sense' their environment and respond accordingly. Cell-ECM interactions occur through adhesions and are mediated by transmembrane proteins called integrins, which, depending on the ECM properties, can recruit, directly or indirectly, >200 proteins and transduce external signals to intracellular chemical signals. However, how adhesions assemble, grow, and disassemble is poorly understood. Here, using a differential equation-based mechano-chemical computational model, we investigate how substrate stiffness influences adhesion formation, maturation and disassembly. We explicitly include the role of talin and vinculin-based reinforcement in these processes. The model we present is robust and can be fine-tuned for particular cell-types and signalling mechanisms. The simulations predict the highest amount of maturation on substrates of an intermediate, 'optimum' stiffness, and that (dis)assembly rates need to change dynamically for cells to establish this 'optimum'. In summary, our results highlight the importance of vinculin availability in adhesion maturation and reinforcement and aid our understanding of cell adhesion formation and mechanotransduction.

Introduction

Direct contact between cells and the extracellular matrix (ECM) through adhesions is a crucial component of multicellular organisms [1]. Integrins are transmembrane ECM receptor proteins that assemble as non-covalently bonded heterodimers with α and β subunits [2]. The integrin ectodomain binds ECM ligands while the cytoplasmic tail is indirectly linked to the actomyosin cytoskeleton of the cell forming a supramolecular assembly or 'clutch' [3–6]. This indirect link consists of a dynamic network of over 200 proteins, collectively termed the 'integrin adhesome' [7, 8]. Central to integrin function are the dynamics and balance of extra- and intracellular forces [9] which drive the force-dependent evolution of the integrin adhesion complexes (IACs) [7] leading to changes in their size and composition. *In vitro* studies have shown that adhesion assembly is a multi-step process where integrins are first activated by binding to intracellular adaptor protein molecules such as talin [10–12] and/or to an ECM ligand [13]. Once activated, integrins cluster at the site of adhesion, independent of force and substrate rigidity, to form nascent adhesions (NAs) [14–16]. Then, NAs either undergo disassembly or force-dependent maturation by the recruitment of other adaptor proteins such as vinculin, to form focal adhesions (FA) (Fig 1A) [17, 18]. These three major steps of adhesion assembly also overlap in time and are not strictly sequential. Understanding interactions between key proteins of the integrin adhesome and force generation will provide valuable insight into cell-ECM interactions, with consequences for developmental biology. A better understanding of cellular responses and signalling can potentially highlight new therapeutic targets, and improve engineered substrates to better mimic biological tissue, thus advancing regenerative medicine.

In addition to questions pertaining to adhesion (dis)assembly, adhesion maturation is also a complex process influenced by the mechanical properties of the substrate [19, 20], force-dependent conformational changes [21–25], different catch and slip bond strengths [5, 26, 27] and intracellular forces [20, 28, 29]. How changes in these mechanical factors affect the
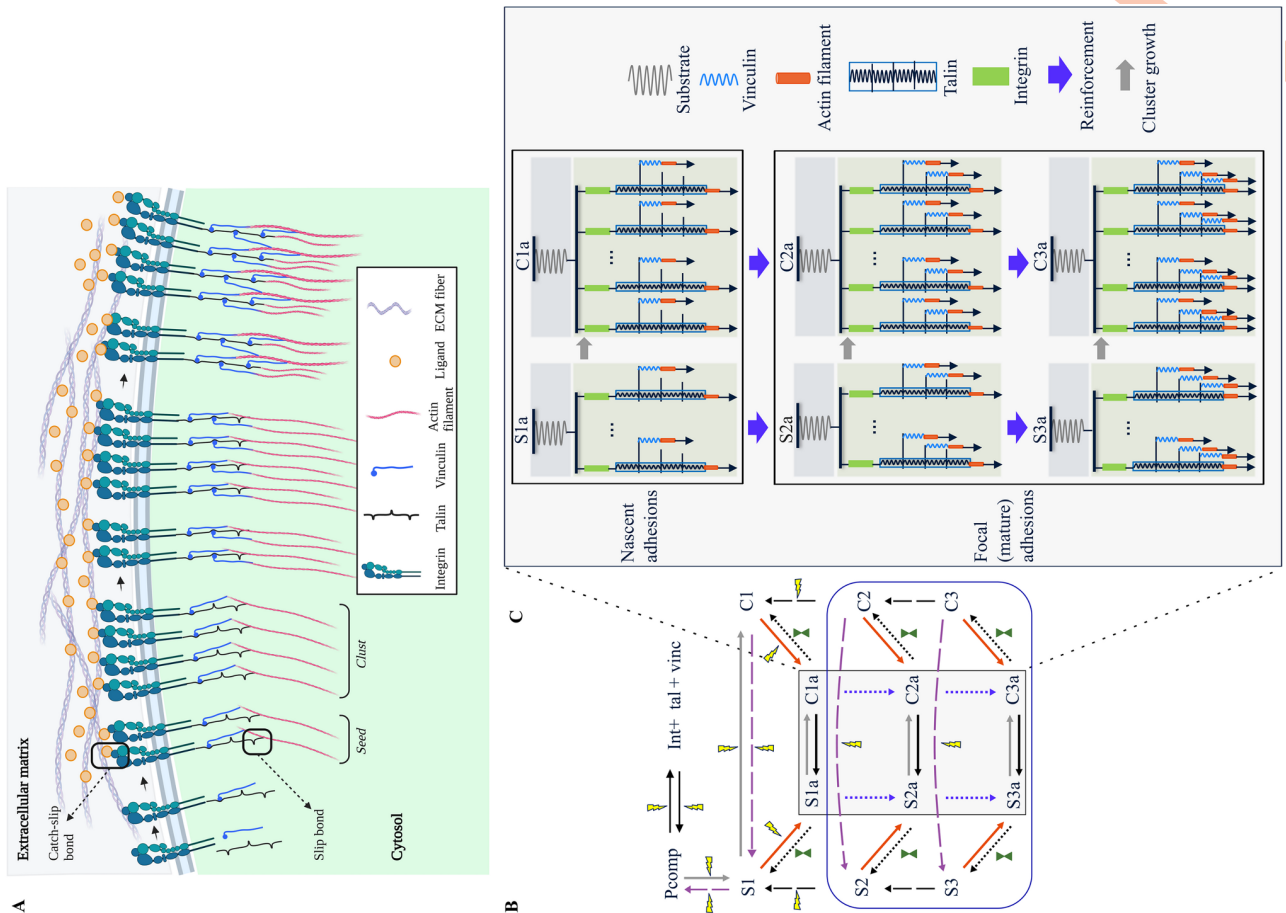
Fig 1. Overview of the processes modelled in this study. (A)—Integrins bind to talin and vinculin in a precomplexation step, then form a small cluster, termed 'seed'. Seeds can dimerise to form larger clusters, termed 'clusts'. Actin filaments pull on talin and vinculin causing cryptic vinculin-binding sites on talin to be exposed, promoting more vinculin recruitment. This chain can then break at the integrin–ligand catch-slip bond or the talin–actin slip bond (black boxes). See Table 1 for a detailed description of the terminology. (B)—Overview of reactions in the model. Int, tal, and vinc refer to concentrations of integrins, talin and vinculin respectively. Black rectangle encloses the reinforcement reactions (expanded further in Fig 1C). Grey arrows represent clust formation reactions. Red arrows represent actin binding reactions. Dotted arrows represent force-dependent reactions—blue dotted: reinforcement, black dotted: actin unbinding. Dashed arrows represent adhesion disassembly reactions, black dashed: talin refolding, purple dashed: cluster breakdown. Yellow lightning bolts indicate rates that undergo signal-dependent rate modification (SDRM), dark green solid hourglasses represent rates that undergo time-dependent rate modification (TDRM). The rate constants undergoing signal-dependent modifications are driven to zero after $\sim$158 s leaving active only the lower part of the model, enclosed in the blue box, representing adhesions that will undergo further maturation. (C)—Talin and vinculin are modelled as Hookean springs (also see Fig A in S1 Appendix). In this model, to capture the process of reinforcement, a maximum of three vinculin binding events occur sequentially (blue arrows) at different points along the talin rod, thereby increasing the stiffness of individual integrin–talin–vinculin spring systems. Clustering is modelled as an increase in the number of integrin–talin–vinculin spring systems in parallel (grey arrows). This figure was created using BioRender.com.

https://doi.org/10.1371/journal.pcbi.1011500.g001

biochemical composition of adhesions, and which factors determine the decision to mature a particular NA remains unclear.

Given the constraints and challenges of experimental studies, computational modelling can be a valuable resource. Many computational models of cell–ECM interactions have been developed since the first molecular-clutch model by Chan and Odde (2008) [4] that explained filopodial traction dynamics on compliant substrates [30–34]. Elosegui-Artola and colleagues have extended the Chan and Odde model to include adhesion reinforcement through increases in integrin density [35] and multiple integrin types [36]. Integrin-based Rho signalling [34] and reversible cross-links in the actin filament network [37] have also been included

in previous studies by other groups. More recently, Venturini and Saez (2023) [38] have developed an extensive multi-scale model of molecular clutch-driven adhesion mechanics. All these models explore adhesion formation, growth, and the influence of substrate stiffness and actomyosin forces on traction forces, but they are discrete models that simulate a relatively small number of individual particles. They also do not account for the increase in clutch stiffness after the recruitment of vinculin and do not consider the disassembly processes to be dynamic and active. In addition, these models give little information about the changes to the overall biochemical composition of adhesions in the cell during the process of maturation of NAs to FAs.

In this study, we developed a new model using ordinary differential equations (ODEs) to describe the biochemical composition of cell–ECM adhesions over time based on mechanical properties like substrate stiffness, adaptor protein stiffness, actomyosin-generated forces, and bond characteristics. Using our model, we studied the fraction of NAs that have the potential to become mature FAs under different mechanical circumstances. Overall, the results from this study shed light on the mechanotransduction mechanisms underlying adhesion maturation and disassembly. This model also provides a reliable starting point to model the larger focal adhesome with over 200 identified proteins [7].

Methods

Differential equation model

We developed an ODE-based model that captures changes in the biochemical composition of cell–ECM adhesions based on the mechanical properties of the environment and intracellular proteins. Below we shortly describe the particular phases of the adhesion maturation process—formation of integrin-talin-vinculin precomplexes, formation and growth of precomplex clusters, actin binding and unbinding, adhesion reinforcement with vinculin, and adhesion breakdown—and how they are modelled (Fig 1B provides an overview of all the species in the system and their interactions). For each subprocess (in bold), we give a brief explanation and also label the corresponding terms in the differential equations (Eqs 1–17). Unless otherwise mentioned, reactions are reversible with forward rate constants having 'f' in the subscript and reverse rate constants having 'r'. Reactions follow mass-action kinetics unless mentioned otherwise. When referring to concentrations in the text, they are written between square brackets (e.g., [S3a]), and when referred to as a species they are written as is (e.g., S3a). A detailed explanation of the reactions and parameters can be found in Text A and Table A in S1 Appendix. Table 1 provides an overview of the terminology used throughout the manuscript.

Adhesion assembly starts with integrin activation. In this study, we model $\alpha_5\beta_1$ integrins and assume they are activated. We also assume that the ligand spacing on the substrate is sufficiently close for integrin clusters to form.

Pcomp formation and dissociation. Activated integrins, [Int], bind to talin, [tal], and vinculin, [vinc], forming pre-complexes [Pcomp], a necessary step for adhesion maturation [18] (Text A in S1 Appendix).

Seed formation and dimerisation. Up to 50 IAPCs cluster independent of substrate rigidity and tension to form NAs [16]. Here, as a simplification, the growth of clusters to the maximal size (50 IAPCs) occurs in two stages—first, a small cluster of 25 IAPCs, termed 'seed' (denoted by 'Sx' (Fig 1C, Table 1) is formed, and a second stage where seeds dimerise, forming a large cluster with 50 IAPCs, termed 'clust' (denoted by 'Cx' (Fig 1C, Table 1, Text A in S1 Appendix)). Here, $x \in \{1,2,3\}$ denotes the number of vinculin molecules in the individual IAPCs.

When a clutch is AUB, the stretched talin is likely to refold [24, 39]. We assume this makes it very unlikely for AUB seeds of mid- and high- order (S2, S3) to dimerise. AB seeds of all

Table 1. Terminology used in this manuscript.

Term	Description
Integrin-Adaptor Protein Complex (IAPC)	Assembly of integrin, talin and vinculin. Three possible IAPCs with talin bound to one, two, or three vinculin molecules are considered.
Pcomp	A pre-complex—an individual IAPC with talin bound to a single vinculin molecule.
Seed—(Sx)	A cluster of 25 IAPCs bound parallelly (Fig 1C). Denoted by Sx, where x is the number of vinculin molecules bound to talin in each IAPC that makes up the seed, ($x \in \{1, 2, 3\}$).
Clust—(Cx)	A cluster of 50 IAPCs bound parallelly (cluster size taken from [16]) (Fig 1C). Denoted by Cx, where $x \in \{1, 2, 3\}$ is the number of vinculin molecules bound to talin in each IAPC that makes up the clust.
Order—($x \in \{1, 2, 3\}$)	The order of a seed/clust is indicative of the number of vinculin molecules bound to talin in each IAPC that makes up the seed/clust. Low, mid and high order seeds/clusts refer to seeds/clusts made of IAPCs containing one, two or three vinculin molecules respectively.
Clutch	An umbrella term that refers to a supramolecular assembly of integrins and adaptor proteins that can function as a molecular clutch between the substrate and the cell (Fig 1C). In this model, both seeds and clusts are capable of this function.
Actin Bound (AB)—(Sxa, Cxa)	Talin and vinculin have actin-binding sites allowing clutches to bind to actin, experience a force and, consequently, an extension. Seeds and clusts that are bound to actin are said to be actin bound (AB). Denoted by Sxa and Cxa respectively ($x \in \{1, 2, 3\}$).
Actin Unbound (AUB)	The talin–actin and vinculin–actin bonds break at certain force thresholds resulting in the clutches being unbound from actin. These are actin unbound (AUB) clutches. Denoted by Sx and Cx ($x \in \{1, 2, 3\}$). AUB clutches do not experience any force or extension.

orders (S1a, S2a, S3a) can dimerise to form AB clusts (C1a, C2a, and C3a) (grey arrows in Fig 1B).

Actin binding/unbinding. Actin-unbound (AUB) seeds and clusts can bind to actin through the actin-binding sites on talin and vinculin, giving AB seeds and clusts (denoted by 'Sxa' and 'Cxa' respectively, (Text A in S1 Appendix)) that can stretch to different extents (based on the value of x) and hence transmit varying magnitudes of force (Fig 1C).

While the baseline actin-binding rate is k_{act} for all actin-binding reactions, signalling molecules such as focal adhesion kinase (FAK), Src and ERK play a role in adhesion turnover, and their inhibition leads to more maturation [40]. To implement a similar mechanism to stop indefinite adhesion formation and maturation, we introduce in the model a signal-dependent rate modification (SDRM) (see 'Signal dependent rate modification (SDRM)' for details).

Depending on the force on the integrin-ligand (catch-slip) bonds [41] and the talin-actin (slip) bonds [5], the force-chain between the cell and the substrate can break at either of these bonds. We capture these phenomena through force-dependent (and consequently substrate rigidity-dependent) actin unbinding rates (black dotted arrows in Fig 1B, also see Text A in S1 Appendix for details). These bonds may also rupture due to random thermodynamic fluctuations before the clutches can reach their maximum force-carrying capacity, reducing the total force exerted by the clutches. To account for the spontaneous clutch unbinding in a continuous framework, we introduce a time-dependent rate modification (TDRM) (see 'Force-dependent actin-unbinding and time-dependent rate modification (TDRM)' for details).

Reinforcement. The AB clutches form a mechanical link between the substrate and the actin cytoskeleton, enabling force transmission and protein unfolding. Up to eleven cryptic vinculin-binding sites (VBS) are uncovered when talin is stretched and unfolded [42, 43],

leading to reinforcement by vinculin recruitment. The rate of talin unfolding and reinforcement occurring depends on the force experienced by the AB clutch, and increases with increasing force, similar to the Bell model [24, 44, 45] (for more details see section 'Adhesion reinforcement rates'). In this simplified model, two vinculin-reinforcement events are considered, one from low- to mid-order clutches (S1a to S2a and C1a to C2a), followed by one from mid- to high-order clutches (S2a to S3a and C2a to C3a) (see Text A in S1 Appendix for a detailed explanation). Thus, in this model, the talin rod can be bound to at least 1 and at most 3 vinculin molecules. With this framework, we consider low-order clutches (S1, S1a, C1, C1a (Fig 1C)) to represent NAs, and mid- and high-order clutches (S2, S2a, C2, C2a, S3, S3a, C3, C3a, (Fig 1C)) to represent more mature stages of adhesions, indicative of the fraction of NAs that mature into FAs (see Section 'NA formation is rigidity- and force-independent' for reasoning). Reinforcement is modelled as a single-step reaction where simultaneous recruitment of 25 (for seeds) and 50 (for clusts) vinculin molecules respectively occurs (indicated by blue dotted arrows in Fig 1B). The order of these reactions with respect to vinculin, however, was chosen to be 2 (Eqs 3, 8, 9 and 10), to account for the effects of possible intermediate stages in the reactions.

Refolding and breakdown.   In the absence of sufficient force, adhesions disassemble because of mechanical and chemical signals [46]. Here, we model two parallel processes of disassembly, namely 1) talin refolding (black dashed arrows in Fig 1B) leading to the loss of vinculin from, and weakening of, clutches, and 2) breakdown of AUB clusters into seeds and Pcomp (purple dashed arrows in Fig 1B) leading to reduced force carrying capacity of the adhesions (Text A in S1 Appendix). These are irreversible reactions.

To account for the mechanical aspects of adhesion assembly, the substrate–integrin–adaptor protein system was formulated as a system of Hookean springs. When clutches bind to the actin filaments, they provide resistance to the motion of actin filaments until bond rupture, caused either randomly or because the catch/slip bond force threshold is reached. We assume that the force exerted by myosin II motors on actin filaments is balanced by the drag force arising due to the viscosity of the cytoplasm. Thus, in the absence of integrin-mediated forces on actin filaments, they move with a constant retrograde velocity (see Text A in S1 Appendix). As a continuous ODE framework is used, we consider the same actin retrograde velocity for all clutches. The force on a clutch depends on its stiffness and extension (according to Hooke's law). The stiffness of a clutch depends on the number of constituent IAPCs and the number of vinculin molecules in each IAPC (equivalent spring constants are calculated, see Text A in S1 Appendix). The total force exerted on the actin filament network thus depends on the number of AB clutches of each type and their stiffnesses. Since we use a continuum approach to account for the abundance of each species, we discretise concentrations of AB clutches by assuming a volume of 1 μm^3 to calculate the total force (see Text A in S1 Appendix).

Together, the above-described processes result in the following set of differential equations:

$$\frac{d[int]}{dt} = \underbrace{-k_{1f} \cdot [int] \cdot [tal] \cdot [vinc] + k_{1r} \cdot [Pcomp]}_{Pcomp \ formation \ and \ dissociation} \tag{1}$$

$$\frac{d[tal]}{dt} = \underbrace{-k_{1f} \cdot [int] \cdot [tal] \cdot [vinc] + k_{1r} \cdot [Pcomp]}_{Pcomp \ formation \ and \ dissociation} \tag{2}$$

$$\frac{d[vinc]}{dt} = \underbrace{-k_{1f} \cdot [int] \cdot [tal] \cdot [vinc] + k_{1r} \cdot [Pcomp]}_{Pcomp\ formation\ and\ dissociation}$$

$$+ 25 \cdot \left(\underbrace{-k_{7f} \cdot [S1a] \cdot [vinc]^2 + k_{7r} \cdot [S2a]}_{S1a\ \underleftrightarrow{reinforcement}\ S2a} \underbrace{-k_{8f} \cdot [S2a] \cdot [vinc]^2 + k_{8r} \cdot [S3a]}_{S2a\ \underleftrightarrow{reinforcement}\ S3a} \right.$$

$$\left. + \underbrace{k_{17f} \cdot [S3]}_{S3\ \xrightarrow{refolding}\ S2} + \underbrace{k_{18f} \cdot [S2]}_{S2\ \xrightarrow{refolding}\ S1} \right) \tag{3}$$

$$+ 50 \cdot \left(\underbrace{-k_{12f} \cdot [C1a] \cdot [vinc]^2 + k_{12r} \cdot [C2a]}_{C1a\ \underleftrightarrow{reinforcement}\ C2a} \underbrace{-k_{13f} \cdot [C2a] \cdot vinc^2 + k_{13r} \cdot [C3a]}_{C2a\ \underleftrightarrow{reinforcement}\ C3a} \right.$$

$$\left. + \underbrace{k_{19f} \cdot [C3]}_{C3\ \xrightarrow{refolding}\ S2} + \underbrace{k_{20f} \cdot [C2]}_{C2\ \xrightarrow{refolding}\ C1} \right)$$

$$\frac{d[Pcomp]}{dt} = \underbrace{k_{1f} \cdot [int] \cdot [tal] \cdot [vinc] - k_{1r} \cdot [Pcomp]}_{Pcomp\ formation\ and\ dissociation}$$

$$- 25 \cdot \underbrace{(k_{2f} \cdot [Pcomp]^2 - k_{2r} \cdot [S1])}_{Seed\ formation} \tag{4}$$

$$\frac{d[S1]}{dt} = \underbrace{k_{2f} \cdot [Pcomp]^2 - k_{2r} \cdot [S1]}_{Seed\ formation} - 2 \cdot \underbrace{(k_{3f} \cdot [S1]^2 - k_{3r} \cdot [C1])}_{S1\ \underleftrightarrow{dimerisation}\ C1}$$

$$\underbrace{-k_{4f} \cdot [S1] + k_{4r} \cdot [S1a]}_{Actin\ binding/unbinding} + \underbrace{k_{18f} \cdot [S2]}_{S2\ \xrightarrow{refolding}\ S1} \tag{5}$$

$$\frac{d[S2]}{dt} = \underbrace{-k_{5f} \cdot [S2] + k_{5r} \cdot [S2a]}_{Actin\ binding/unbinding} + \underbrace{k_{17f} \cdot [S3]}_{S3\ \xrightarrow{refolding}\ S2} - \underbrace{k_{18f} \cdot [S2]}_{S2\ \xrightarrow{refolding}\ S1} + \underbrace{2 \cdot k_{22f} \cdot [C2]}_{C2\ \xrightarrow{breakdown}\ S2} \tag{6}$$

$$\frac{d[S3]}{dt} = \underbrace{-k_{6f} \cdot [S3] + k_{6r} \cdot [S3a]}_{Actin\ binding/unbinding} - \underbrace{k_{17f} \cdot [S3]}_{S3\ \xrightarrow{refolding}\ S2} + \underbrace{2 \cdot k_{21f} \cdot [C2]}_{C3\ \xrightarrow{breakdown}\ S3} \tag{7}$$

$$\frac{d[S1a]}{dt} = \underbrace{k_{4f} \cdot [S1] - k_{4r} \cdot [S1a]}_{Actin\ binding/unbinding} \underbrace{-k_{7f} \cdot [S1a] \cdot [vinc]^2 + k_{7r} \cdot [S2a])}_{S1a\ \underleftrightarrow{reinforcement}\ S2a}$$

$$- 2 \cdot \underbrace{(k_{14f} \cdot [S1a]^2 - k_{14r} \cdot [C1a])}_{S1a\ \underleftrightarrow{dimerisation}\ C1a} \tag{8}$$

$$\frac{d[S2a]}{dt} = \underbrace{k_{5f} \cdot [S2] - k_{5r} \cdot [S2a]}_{Actin\ binding/unbinding} + \underbrace{k_{7f} \cdot [S1a] \cdot [vinc]^2 - k_{7r} \cdot [S2a]}_{S1a\ \overset{reinforcement}{\longleftrightarrow}\ S2a}$$

$$-\underbrace{k_{8f} \cdot [S2a] \cdot [vinc]^2 + k_{8r} \cdot [S3a]}_{S2a\ \overset{reinforcement}{\longleftrightarrow}\ S3a} - 2 \cdot (\underbrace{k_{15f} \cdot [S2a]^2 - k_{15r} \cdot [C2a]}_{S2a\ \overset{dimerisation}{\longleftrightarrow}\ C2a})$$

(9)

$$\frac{d[S3a]}{dt} = \underbrace{k_{6f} \cdot [S3] - k_{6r} \cdot [S3a]}_{Actin\ binding/unbinding} + \underbrace{k_{8f} \cdot [S2a] \cdot [vinc]^2 - k_{8r} \cdot [S3a]}_{S2a\ \overset{reinforcement}{\longleftrightarrow}\ S3a}$$

$$-2 \cdot (\underbrace{k_{16f} \cdot [S3a]^2 - k_{16r} \cdot [C3a]}_{S3a\ \overset{dimerisation}{\longleftrightarrow}\ C3a})$$

(10)

$$\frac{d[C1]}{dt} = \underbrace{2 \cdot k_{3f} \cdot [S1]^2 - k_{3r} \cdot [C1]}_{S1\ \overset{dimerisation}{\longleftrightarrow}\ C1} - \underbrace{k_{9f} \cdot [C1] + k_{9r} \cdot [C1a]}_{Actin\ binding/unbinding} + \underbrace{k_{20f} \cdot [C2]}_{C2\ \overset{refolding}{\longrightarrow}\ C1}$$

(11)

$$\frac{d[C2]}{dt} = \underbrace{-k_{10f} \cdot [C2] + k_{10r} \cdot [C2a]}_{Actin\ binding/unbinding} + \underbrace{k_{19f} \cdot [C3]}_{C3\ \overset{refolding}{\longrightarrow}\ C2} - \underbrace{k_{20f} \cdot [C2]}_{C2\ \overset{refolding}{\longrightarrow}\ C1} - \underbrace{k_{22f} \cdot [C2]}_{C2\ \overset{breakdown}{\longrightarrow}\ S2}$$

(12)

$$\frac{d[C3]}{dt} = \underbrace{-k_{11f} \cdot [C3] + k_{11r} \cdot [C3a]}_{Actin\ binding/unbinding} - \underbrace{k_{19f} \cdot [C3]}_{C3\ \overset{refolding}{\longrightarrow}\ C2} - \underbrace{k_{21f} \cdot [C3]}_{C3\ \overset{breakdown}{\longrightarrow}\ S3}$$

(13)

$$\frac{d[C1a]}{dt} = \underbrace{k_{9f} \cdot [C1] - k_{9r} \cdot [C1a]}_{Actin\ binding/unbinding} - \underbrace{k_{12f} \cdot [C1a] \cdot [vinc]^2 + k_{12r} \cdot [C2a]}_{C1a\ \overset{reinforcement}{\longleftrightarrow}\ C2a}$$

$$+\underbrace{k_{14f} \cdot [S1a]^2 - k_{14r} \cdot [C1a]}_{S1a\ \overset{dimerisation}{\longleftrightarrow}\ C1a}$$

(14)

$$\frac{d[C2a]}{dt} = \underbrace{k_{10f} \cdot [C2] - k_{10r} \cdot [C2a]}_{Actin\ binding/unbinding} + \underbrace{k_{12f} \cdot [C1a] \cdot [vinc]^2 - k_{12r} \cdot [C2a]}_{C1a\ \overleftrightarrow{reinforcement}\ C2a}$$

$$\underbrace{-k_{13f} \cdot [C2a] \cdot [vinc]^2 + k_{13r} \cdot [C3a]}_{C2a\ \overleftrightarrow{reinforcement}\ C3a} + \underbrace{k_{15f} \cdot [S2a]^2 - k_{15r} \cdot [C2a]}_{S2a\ \overleftrightarrow{dimerisation}\ C2a}$$

$$\tag{15}$$

$$\frac{d[C3a]}{dt} = \underbrace{k_{11f} \cdot [C3] - k_{11r} \cdot [C3a]}_{Actin\ binding/unbinding} + \underbrace{k_{13f} \cdot [C2a] \cdot [vinc]^2 - k_{13r} \cdot [C3a]}_{C2a\ \overleftrightarrow{reinforcement}\ C3a}$$

$$\underbrace{+k_{16f} \cdot [S3a]^2 - k_{16r} \cdot [C3a]}_{S3a\ \overleftrightarrow{dimerisation}\ C3a}$$

$$\tag{16}$$

Baseline parameter values and rate constants can be found in Table A in S1 Appendix. We refer the reader to Text A in S1 Appendix for detailed descriptions of all reactions in the model and the underlying reasoning. Below, we highlight the novel methodological approaches (signal- and time-dependent rate modification (SDRM and TDRM)), and provide brief explanations of a few mathematical formulations and assumptions that are used in this model.

Signal dependent rate modification (SDRM)

Nascent adhesions (NAs) form in large numbers and most are disassembled within a time scale of a few minutes [17, 47]. As the cell protrudes, the distance between the cell membrane and the NAs increases, and actin depolymerization rates are higher away from the cell membrane [48]. Thus, numerous NAs may be supported near the cell membrane but in the absence of this scaffold, many NAs disassemble. Various signal cascades also regulate adhesion disassembly. Signalling molecules such as focal adhesion kinase (FAK), Src and ERK kinases play a role in adhesion turnover, and their inhibition leads to more maturation [40]. However, most studies have investigated the effects of signalling molecules on the turnover of FAs and not NAs [49, 50], and the exact mechanical or chemical triggers for NA disassembly remain elusive [51]. NA assembly at the cell front, maturation, and disassembly away from the leading edge occur constantly due to above-mentioned mechanisms. In this study, we focus on one cycle of NA formation and investigated the differences in NA maturation on different substrate stiffnesses. To implement a mechanism to stop indefinite adhesion formation and maturation, it is hypothesized that there exists a signal molecule of which a minimum concentration, $signal_{thresh}$, is required for new NA formation and low-order AUB clutches (S1, C1) to bind actin for maturation. The concentration [signal] of this molecule is initially high and decreases at an arbitrary rate following Michaelis-Menten kinetics given by:

$$\frac{d[signal]}{dt} = \frac{-k_{23_{vmax}} \cdot [signal]}{k_{23_{KM}} + [signal]} \tag{17}$$

Initial estimates for values of the maximum velocity $k_{23_{vmax}}$ and the Michaelis constant $k_{23_{KM}}$ were based on those reported in the literature for FAK Tyr-397 phosphorylation in the presence of ATP [52] but were adjusted such that the concentration of [signal] reaches the $signal_{thresh}$ in 58 s, which is the approximate duration of the NA assembly phase as measured in experiments [4]. When the [signal] falls below $signal_{thresh}$, it is analogous to a signalling pathway being

activated, and particular reaction rate constants (k_{1f}, k_{1r}, k_{2f}, k_{2r}, k_{3f}, k_{3r}, k_{4f}, k_{9f}, k_{18f}, k_{20f}, k_{21f}, k_{22f}, indicated by yellow lighting bolts in Fig 1B) are modified as detailed in Text A in S1 Appendix. Thus, the rate of decay of [signal] determines the amount of time available before NA disassembly starts in which adhesion maturation can occur. Note that the model behaviour does not change if we assume the opposite i.e., [signal] increases over time and there is an upper limit for its concentration beyond which actin binding does not occur (Fig C.B in S1 Appendix).

Force-dependent actin-unbinding and time-dependent rate modification (TDRM)

A cell–ECM force chain is broken if either the integrin–ligand (catch-slip) bond [41] or the talin–actin (slip) bond [5] ruptures as a result of reaching the respective force thresholds or due to random thermodynamic fluctuations. This is described in detail in Text A in S1 Appendix. To capture the combined dynamics of the catch-slip and slip bonds, as well as the effect of random bond ruptures, the actin unbinding rates (dark green hourglasses in Fig 1B) are defined as follows:

$$\{k_{4r}, k_{5r}, k_{6r}, k_{9r}, k_{10r}, k_{11r}\} = A \cdot e^{-b \cdot F_{clutch}} + C \cdot e^{d \cdot F_{clutch}} + k_{TDRM} \cdot k_{slip_{UL}} \cdot e^{\frac{F_{clutch}}{F_{th_i}}} \quad (18)$$

where F_{clutch} is the force on an individual IAPC in the clutch (see Text A in S1 Appendix where F_{clutch} is described in detail). The first and second terms, where A and C are scaling factors and b and d control the force-dependency, describe the integrin–ligand catch-slip bond, and the third term describes the talin-actin slip bond where F_{th_i} is bond rupture threshold for a given clutch type ($i \in \{1, 2, 3\}$, refer Table A in S1 Appendix) and $k_{slip_{UL}}$ is the unloaded dissociation rate. k_{TDRM} is the time-dependent rate modification (TDRM) factor that is required to qualitatively account for the reduction in the total force caused by spontaneous clutch unbinding events. k_{TDRM} is given by:

$$k_{TDRM} = 1 + k_{sens} \cdot t_{clutch} \cdot dt \quad (19)$$

where t_{clutch} is the number of simulated time-steps that a clutch remains actin-bound, dt is the time-step and k_{sens} is a parameter that determines the magnitude of the influence. In short, this definition captures the decreasing likelihood of an AB clutch remaining AB for long periods of time. It has been shown that integrin-ligand bonds undergo cyclic mechanical reinforcement (CMR) leading to longer lifetimes [53]. This implies that on soft substrates where the force-loading rate is low, integrin-ligand bonds experience fewer force cycles in a given time period compared to stiff substrates and consequently are more likely to break on soft substrates. Previous studies model CMR with an increased bond-dissociation rate at low forces [35, 38]. Here, TDRM can capture the effects of these phenomena. TDRM affects softer substrates, where clutches take longer to reach their force thresholds, more than stiff substrates.

When an AB clutch experiences a force equal to its force threshold, it unbinds from actin and becomes an AUB clutch. Thus, the concentration of the AB clutch is set to 0, and the concentration of its AUB counterpart is increased by the same amount.

Adhesion reinforcement rates

The rate at which the talin rod unfolds increases with applied force and has been described in previous studies by the Bell model [24, 44, 45]. Here, the Bell formulation was adapted such that the rate increases exponentially with force until the vinculin binding force threshold F_{vb} is

reached, beyond which it remains constant. The rate is given by:

$$
k_{unfold} = \begin{cases} k_{unfold_{UL}} \cdot e^{k_{UF} \cdot \frac{F_{clutch}}{F_{vb_i}}} & \text{if } F_{clutch} \leq F_{vb_i} \\ k_{unfold_{UL}} \cdot e^{k_{UF}} & \text{if } F_{clutch} > F_{vb_i} \end{cases} \tag{20}
$$

where $k_{unfold_{UL}}$ is the rate of unloaded talin unfolding, k_{UF} is a parameter controlling force-dependence, F_{clutch} is the force experienced by an individual IAPC in the clutch, and F_{vb_i} is the vinculin binding force threshold, with $i \in \{1, 2\}$ corresponding to the first and second vinculin binding steps. Here, $F_{vb_1} = 5$ pN and $F_{vb_2} = 12$ pN [24, 42]. Vinculin binding is assumed to occur instantaneously once the VBS is uncovered [45, 54], and hence the rates of reinforcement were determined based on the force-dependent unfolding kinetics of talin as observed in single-molecule experiments using magnetic tweezers [42]. A detailed description of the method used for curve-fitting can be found in Text A in S1 Appendix.

Range of substrate rigidities

The stiffness of the ECM, generally measured in terms of Young's modulus, varies across three orders of magnitude, between 1–3 kPa in the brain, 23–42 kPa in muscular tissue, 1000 kPa-860 MPa in blood vessels, to 15–40 GPa in bone [55]. In this study, however, we consider spring constants, which can be converted to Young's moduli based on a few assumptions as detailed in [34, 36] and summarized in Text A in S1 Appendix. Accordingly, we restrict the scope of the main investigations and predictions to a stiffness range equivalent to 0.1–130 kPa and only qualitatively discuss the results up to 1000 kPa. This is in line with previous computational and experimental studies which have also primarily studied adhesion mechanobiology in similar ranges of substrate rigidities [4, 36].

Local sensitivity analysis

As the model included many parameters whose values were either estimated or adapted to fit experimental data, a local sensitivity analysis was performed. The range of values tested for each parameter was the baseline value (Table A in S1 Appendix) ±10% and ±20%. To quantify the influence, two different metrics were used as outcomes, namely 1) maturation fraction: the concentration of integrins in mid- and high-order AB and AUB clutches ([S2]+[S2a]+[S3]+[S3a]+[C2]+[C2a]+[C3]+[C3a]) at equilibrium (the last time point), and 2) the optimal stiffness: the substrate stiffness with the lowest mean actin retrograde velocity. Outcome 1 represents the total fraction of integrins in the system that made it beyond the initial force-independent stage of adhesion formation, indicative of the fraction of NAs that mature into FAs. Outcome 2 represents an overall influence on the system as it quantifies the mean force exerted during the length of the simulation for a range of substrate stiffnesses. In addition, cells are known to be able to tune their mechanosensitive ranges to adapt to their environments, an aspect on which outcome 2 can shed light. As different parameters may have different levels of influence based on the substrate stiffness, the sensitivity of outcome 1 to each parameter was evaluated for four substrate stiffnesses (k_{sub} = 0.1, 1, 10, 100 pN/nm).

Parameter sensitivity analysis was performed on 21 parameters (Text B, Fig I and Fig J in S1 Appendix), and the ones with the highest influence or of key importance are presented in the main text. The parameter sensitivity for a parameter p for an outcome i was calculated as

follows:

$$Sensitivity_{p,i} = \frac{|Outcome_i(p + \Delta p) - Outcome_i(p)|}{Outcome_i(p)} \Big/ \frac{\Delta p}{p} \qquad (21)$$

where $Outcome_i(p + \Delta p)$ represents the value of the outcome metric with the changed parameter value, $Outcome_i(p)$ is the value of the outcome metric with the baseline parameter value, and Δp and p are the change in the parameter and the baseline parameter value respectively.

Initial conditions

The initial concentrations of integrins, talin and vinculin were assumed to be equal and set to 1 μM for simplicity, and that of all other species were set to 0. Vinculin was assumed to be abundantly available within the cytoplasm and thus modelled at a constant concentration of 1 μM throughout the simulation.

Simulation steps

All simulations were run for 600 s. Euler's forward integration method was used to solve the ODEs with a time step dt of 5 ms as used in previous computational studies [4, 35]. For mass conservation steps, see Text A in S1 Appendix. The steps of integration and the order of updates (Fig 2) of the different aspects of the model are as follows:

1. Force-dependent rate constants are calculated. In particular, the following rates are evaluated at the current force:

   a. First reinforcement rates: (k_{7f}, k_{12f}) using Eq 20.

   b. Second reinforcement rates: (k_{8f}, k_{13f}) using Eq 20.

   c. Signal-dependent rate modification: (k_{1f}, k_{1r}, k_{2f}, k_{2r}, k_{3f}, k_{3r}, k_{4f}, k_{9f}, k_{18f}, k_{20f}, k_{21f}, k_{22f}) are updated as detailed in Text A in S1 Appendix.

   d. Catch-slip bond rates with time-dependent rate modification: (k_{4r}, k_{5r}, k_{6r}, k_{9r}, k_{10r}, k_{11r}) using Eqs 18 and 19.

2. Concentrations are updated based on current rate constants by solving the differential equations listed above.

3. The slip bond threshold is checked for each clutch type

   a. If the slip bond threshold is reached, the force on the clutch is reset to 0.

   b. The concentration of the actin-bound form of the clutch is converted to the actin-unbound form.

4. The total force exerted by actin-bound clutches is calculated based on discretised concentrations using eq. S53.

5. Retrograde velocity, v_{retro}, is updated based on the current total force in the system using eq. S49.

6. All substrate-clutch spring systems are extended by an amount $v_{retro} \cdot dt$.
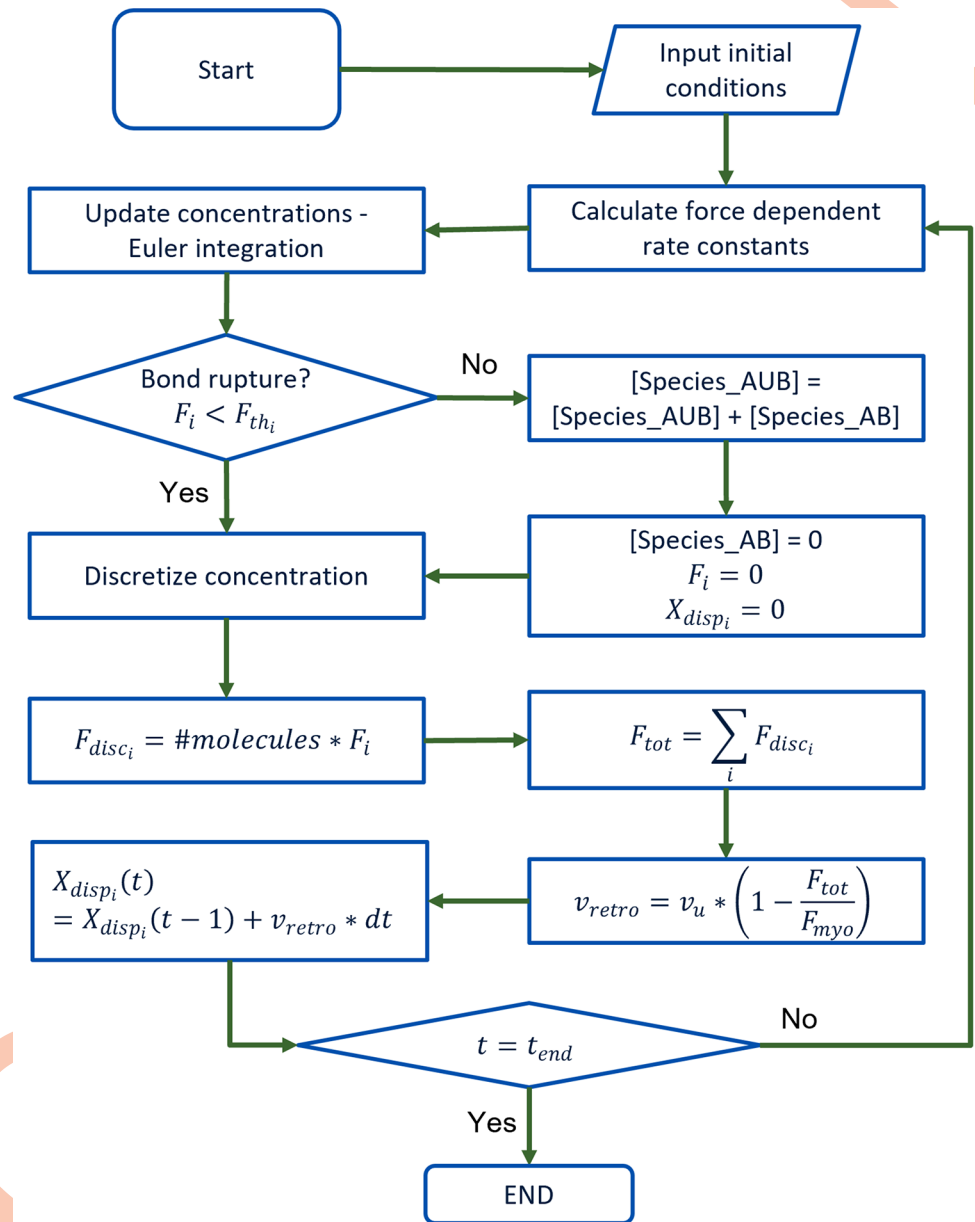
7. Force on each clutch is updated using eq. S51.

Fig 2. Schematic showing the flowchart for simulation and force quantification.
https://doi.org/10.1371/journal.pcbi.1011500.g002

Results

To explore the influence of mechanical properties like substrate stiffness, adaptor protein stiffness, actomyosin-generated forces and bond characteristics on adhesion maturation, we developed a computational model that captures the overall changes to the IAC compositions as adhesions form and mature. The model, based on ODEs, consists of a single compartment that represents a patch of the cell where adhesions form, and considers three core components: integrins, talin and vinculin, from which 14 other species are made. The dynamic NA/FA maturation is modelled by a total of 22 reactions (explained in Methods and Text A, Tables A and

B in S1 Appendix) that largely represent three distinct processes (Fig 1): (i) adhesion formation, (ii) reinforcement and growth, and (iii) adhesion disassembly.

Using our mechanochemical computational model, we find that dynamic rates of assembly and disassembly, which are likely regulated by biochemical signalling events, are essential to determine the subset of NAs that mature. The model was found to satisfy mass conservation (Text B, Fig B in S1 Appendix).

NA formation is rigidity- and force-independent

When only pre-complex, initial seed and clust formation reactions (Rx1, Rx2 and Rx3) were active (see Text B, Table B in S1 Appendix) the concentration of seeds and clusts for all substrate stiffnesses tested were equal, in line with previous experimental evidence showing that NA formation is substrate rigidity-independent [16] (Fig 3A). This is the result of the rigidity- and force-independent rate constants (k_{1f}, k_{1r}, k_{2f}, k_{2r}, k_{3f}, k_{3r}) for reactions Rx1, Rx2 and Rx3. Thus, the concentration of seeds and clusts formed only depends on the initial concentrations of [int], [tal], and [vinc], which were all set to 1 μM, with [vinc] being constant throughout the simulation (see Methods).

The baseline signal decay parameters (Table A in S1 Appendix) were set to match experimentally measured time periods for the assembly phase of NAs [17], leading to the concentration of signal crossing the $signal_{thresh}$ at t_{sig} = 58.04 s (Fig 3A, Fig C and Text B in S1 Appendix). Additionally, when maturation (actin-binding) reactions were disabled, the predicted concentration of integrins in seeds and clusts was ≥ 0.1 μM (Fig 3A) for approximately 158 s, a duration indicative of the lifetime of nascent adhesions and is in line with experimentally measured average lifetimes of NAs of 135–180 s [16, 17, 47]. Additionally, the concentrations of [S1] and [C1] also matched experimentally observed trends in abundance of early NAs [17] (Fig 3A).

When actin-binding reactions were allowed however, the concentration of [S1a] and [C1a] reached a peak at 58 s (Fig 3B), followed by a sharp fall to 0. This decrease is because the signal-dependent reduction in actin-binding rates reduced the formation of these species, but the
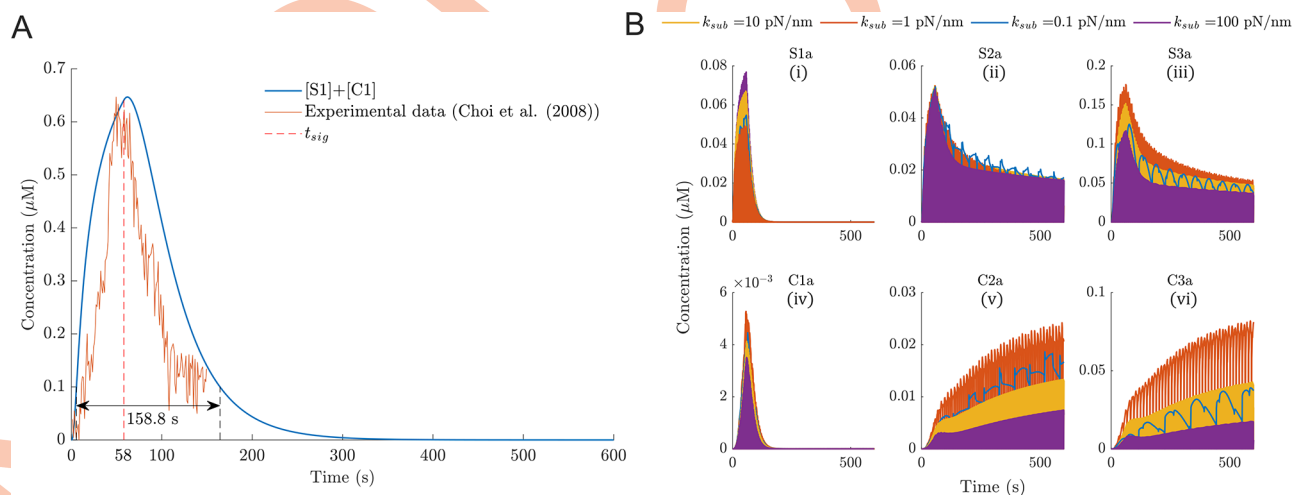

Fig 3. While NA formation is substrate stiffness independent, maturation is influenced considerably by stiffness. (A)—Concentration over time of species in the model that represent NAs (S1 and C1). The curves for all tested substrate rigidities overlap and hence appear as a single (blue) line. The vertical dotted line marks the time point when the signal threshold is crossed and hence new NA formation reduces. (B)—Concentrations over time of all the actin-bound species. Species representing NAs (S1a, C1a) increase initially before being driven to 0 after the signal concentration drops below the threshold. The highest levels of maturation occur on substrate of moderate stiffness (k_{sub} = 1 pN/nm).

rate constants (k_{7f} and k_{12f}) of reinforcement reactions, Rx7 and Rx12, that transform S1a and C1a to S2a and C2a, respectively, remained unchanged. Thus, S1a and C1a were almost completely consumed after approximately 158 s. The predicted concentrations of [S1a] and [S3a] are highest on k_{sub} = 100 pN/nm and k_{sub} = 1 pN/nm substrates respectively (Fig 3B), whereas [C1a] and [C3a] are always higher on k_{sub} = 1 pN/nm. These differences arise from the stiffness-dependent reinforcement rates, and the reversible mass-action kinetics considered here. This is explained in more detail in Text B in S1 Appendix. As such, the model accounts for one cycle of NA assembly, followed by either maturation or disassembly. When maturation was enabled, the concentrations of [S2a], [C2a], [S3a] and [C3a] reach a steady state after 600 s, in that they oscillate between 0 and an almost constant peak concentration (Fig 3B). In summary, the balance between the reversible mass-action kinetics, stiffness-dependent reinforcement rates, and signal concentration decay results in the formation and subsequent disassembly of low-order species (S1, C1, S1a, C1a) representing NAs, while mid- and high-order species (S2, C2, S2a, C2a, S3, C3, S3a, C3a) represent stable adhesions that may further mature to become FAs.

Adhesion maturation is highest on moderate substrate stiffness

The concentrations of [S3a], [C2a] and [C3a] are highest on a moderate substrate stiffness (1 pN/nm), and lower on stiffer or softer substrates (Fig 3B) in accordance with experimental findings [4, 34, 56, 57]. This is a result of the time taken for the force on a clutch to reach the bond-rupture threshold being roughly equal to the lifetime of an unloaded AB-clutch that spontaneously dissociates from actin (or the substrate) due to thermodynamic fluctuations [4, 58]. Thus, the lifetime of a complete ECM-integrin-adaptor protein actin chain is maximized, resulting in more maturation. In addition, in the early periods of the simulations (0 to 70 s, Fig D in S1 Appendix), the concentrations [C3a], [C2a] and [S3a] increase most rapidly on k_{sub}=1 pN/nm. While these results are for simulations with a constant vinculin concentration, similar results were obtained for limited vinculin conditions (see Text B and Fig E in S1 Appendix).

Although the concentration plots in Fig 3B are oscillatory due to the repeated bond-rupture events that transform AB clutches to AUB clutches, pushing the concentration of AB clutches to 0 and causing a spike in the concentration of AUB clutches, the peaks approach a steady state. We observed generally shorter periods of oscillations for AB clutches on stiffer substrates (Table 2), which is also reported by Venturini and Saez (2023) [38]. The periods predicted in our simulations were in good agreement with previous studies (Table 2) [4, 38, 58, 59]. Note that the periods for C2a and C3a on k_{sub} = 0.1 pN/nm, are of the order of the lifetime of NAs ($\sim$60 s) or higher. Thus, these results suggest that C2a and C3a can represent (partially) mature adhesions and not NAs, and that adhesions are likely to disassemble before sufficient reinforcement can occur on very soft substrates.

In essence, after the initial NA formation phase, the number of mature adhesions grows, most rapidly on a moderate substrate stiffness of k_{sub} = 1 pN/nm, and approaches a steady

Table 2. Mean periods in s of different actin-bound clutches for different substrate stiffnesses.

Substrate stiffness (pN/nm)	S1a	S2a	S3a	C1a	C2a	C3a
0.1	15.37	32.72	55.74	30.43	64.83	110.48
1	2.01	4.22	7.15	3.67	7.76	13.18
10	0.47	0.94	1.58	0.62	1.26	2.13
100	0.31	0.61	1.02	0.33	0.64	1.07

https://doi.org/10.1371/journal.pcbi.1011500.t002

state. While the number of adhesions actively bound to the actin network constantly fluctuates due to force thresholds being reached or stochastic bond-rupture events, on average the number approaches a stable steady state.

Traction force is highest on substrates of moderate stiffness

An optimal substrate stiffness is one at which the highest traction force is generated at the adhesions [60]. As explained in the previous section, this arises due to a balance between the lifetime of an unloaded AB clutch and the time taken for a clutch to reach the force threshold. In our simulations, the highest traction force was reached at $k_{sub} = 1$ pN/nm, which also corresponded to the point where the lowest retrograde velocity was recorded (Fig 4A). The frequency of oscillations was higher for stiffer substrates (Table 2) given that the force on clutches increases faster on stiff substrates, thus reaching the force thresholds earlier, causing bond-rupture, and subsequent rebinding of the AUB-clutches to actin. While on softer substrates the force build-up is much slower as the substrate is more compliant (hence the lower oscillation frequency), actin unbinding due to thermodynamic fluctuations dominates as bonds break spontaneously much before the force thresholds are reached, giving rise to a higher actin unbinding rate (Fig F in S1 Appendix). These results suggest that $k_{sub} = 1$ pN/nm gives rise to a 'load-and-fail' regime where clutches are loaded at a moderate rate, reach their force thresholds and subsequently break, 'frictional slippage' occurs on stiffer substrates where rapid loading causes clutches to disengage too quickly, resulting in lower average AB-clutch concentration [4, 60]. Altogether, these observations show that the optimal stiffness for NA maturation in our model is at $k_{sub} = 1$ pN/nm.

Fig 4A shows the agreement between the mean retrograde velocity in our simulations and other computational [36, 38] and experimental [4] studies. A recent computational study also reports a similar biphasic behaviour with an optimal stiffness of around 10 pN/nm [38]. However, this is only observed when the weakest link in the force chain in their model is simulated

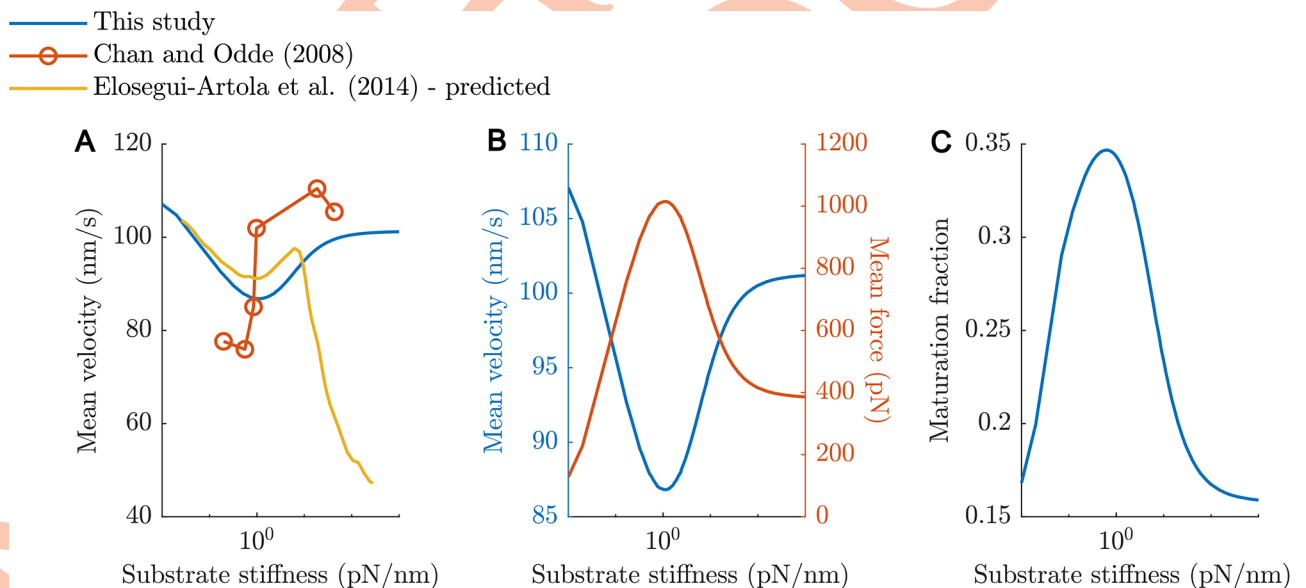Fig 4. Model predictions of mean actin retrograde velocity and maturation fraction for the baseline model. (A) shows the predicted velocity vs substrate stiffness compared to previous studies, (B) shows the predicted velocity (blue) and mean force exerted by all adhesions (red) in this model, and (C) shows the NA maturation fraction vs substrate stiffness.

https://doi.org/10.1371/journal.pcbi.1011500.g004

as a catch bond. Additionally, our model predicts a linear increase in the mean velocity between 10^0 pN/nm and 10^2 pN/nm (Fig 4B), which is the stiffness range where the cell is mechanosensitive—a change in stiffness translates linearly into a change in actin retrograde velocity. This is in good agreement with previous studies which report ranges of 10^0–10^1 to 10^0–10^2 pN/nm [4, 57, 61]. The decrease in the predicted retrograde velocity for stiffnesses $> 10^1$ pN/nm in the computational study of Elosegui-Artola et al. [36] (Fig 4A) arises because of reinforcement which they model as an increase in integrin density beyond a certain threshold force on a clutch. While the range of velocities reported varies, in our model, the lowest velocity depends on the concentration of myosin motors $conc_{myo}$, which is a free parameter that was adjusted such that the lowest velocity was within 10% of that reported by Chan and Odde (2008) [4].

It is also important to note that the optimal stiffness of 1 pN/nm is reached only when the TDRM of actin-unbinding rates was applied (see subsection 'Force-dependent actin-unbinding and time-dependent rate modification (TDRM)' in Methods and Text A in S1 Appendix). For high substrate stiffnesses, since the time taken to reach the force thresholds is short, maturation is limited. For soft stiffnesses, however, this is not the case. Hence, in the absence of TDRM, a method we use to account for the force-independent spontaneous bond ruptures, the equilibrium concentrations of mid- and high-order AB clutches ([S2a], [S3a], [C2a], [C3a]) are highest on k_{sub} = 0.1 pN/nm and decrease monotonically with increasing substrate stiffness (Fig G in S1 Appendix). Importantly, the decrease in equilibrium concentrations of mid- and high-order AB clutches caused by TDRM is the largest on k_{sub} = 0.1 pN/nm and least on k_{sub} = 100 pN/nm (Figs G.A and G.B in S1 Appendix). Thus, TDRM of disassembly rates is essential for obtaining an optimal stiffness through mechanosensing. As adhesion assembly and disassembly are tightly regulated processes, these results suggest altering factors affecting adhesion disassembly allows for more robustness and resilience in the mechanosensing and adhesion maturation processes.

Predicted NA maturation fraction is most sensitive to talin stiffness and vinculin availability

After identifying species in the model that represent NAs (S1, C1, S1a, C1a) and adhesions that mature to FAs (S2, C2, S2a, C2a, S3, C3, S3a, C3a) based on comparisons of their concentrations, bond formation and rupture times to values reported in literature, we used our model to predict the fraction of NAs that may mature into FAs on a range of substrate stiffnesses. Notably, our model also predicts a biphasic trend in maturation fraction (MF) (Fig 4C). More specifically, the MF ranges from approximately 18% on very soft substrates (10^{-2} pN/nm) to around 34.3% on the optimal substrate stiffness of 10^0 pN/nm, which lies within experimentally determined ranges of MFs under different conditions [18, 62].

To ensure that both the optimal stiffness and MF predictions were not heavily influenced by the choice of parameter values, we performed a local sensitivity analysis on 21 parameters (Text B, Figs I and J in S1 Appendix), and address the most important and representative ones here.

The optimal substrate stiffness, the stiffness at which the lowest mean retrograde velocity is observed (Fig 5B), was most sensitive to changes in k_{tal}, the stiffness of talin. Increasing k_{tal} shifts the optimum stiffness to softer substrates and reduces the MF (Fig 5B). Talin is the most abundant mechanosensitive component in the model and majorly contributes to determining the stiffness of clutches, which effectively determines the optimum substrate stiffness. Increasing the stiffness of talin results in stiffer clutches that reach the bond force thresholds sooner, leaving less time for maturation reactions and consequently lower MF.
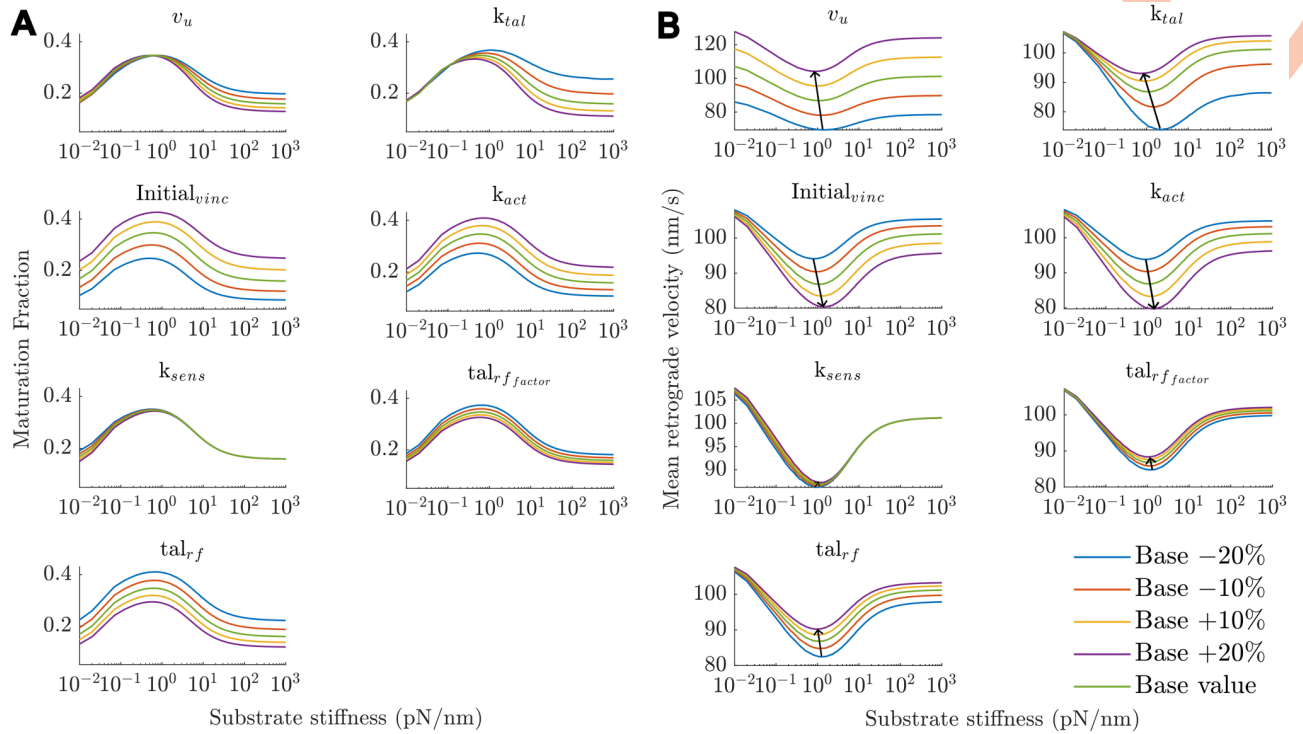
Fig 5. Sensitivity analysis results. (A)—Maturation fraction vs stiffness (outcome 1) and (B)—Mean retrograde velocity vs stiffness for a local variation in parameter values of different parameters. Black arrows in (B) point in the direction of increasing parameter value and track the optimal stiffness (outcome 2).

https://doi.org/10.1371/journal.pcbi.1011500.g005

Increases in initial vinculin concentration $Initial_{vinc}$ leads to large increases in MF (Fig 5A) and small increases in the optimal stiffness (Fig 5B). A higher vinculin concentration increases the likelihood of maturation leading to increased force-carrying capacity and consequently a shift of the optimal stiffness to stiffer regimes. In contrast, a lower vinculin availability leads to decreased maturation fractions and traction force and a higher mean retrograde velocity (Figs 5 and 6).

Changes in the talin refolding rate, tal_{rf}, affect the mean retrograde velocities more than the optimum stiffness (Fig 5). A higher tal_{rf} leads to lower maturation fractions but has negligible effects on the optimum stiffness. This is because a higher talin refolding rate causes AUB clutches unbinding from vinculin more likely and hence lowers the concentration of more mature, higher force-carrying-capacity clutches on all substrate stiffnesses. This, however, does not cause any changes in the relative proportions of concentrations of different clutches across substrate stiffnesses and hence does not change the optimum stiffness considerably. A similar reasoning is valid for a lower tal_{rf}.

The talin refolding factor, $tal_{rf_{factor}}$, controls the rate of vinculin-dissociation and hence relative additional stability of higher order species in our model (see Text A in S1 Appendix) and its baseline value is set to 0.5 in our simulations (talin in higher order species is half as likely to refold compared to mid-order species). Increasing $tal_{rf_{factor}}$ results in lower MFs and shifts the optimal stiffness to softer substrates due to the decreased 'additional' stability of higher-order species. Similar reasoning can be used to explain the effects of decreasing $tal_{rf_{factor}}$. As vinculin is known to 'lock' talin in the unfolded conformation [39], we further reduced the value of $tal_{rf_{factor}}$ to 0.2 to investigate the effects of having highly stable high-order species. This resulted
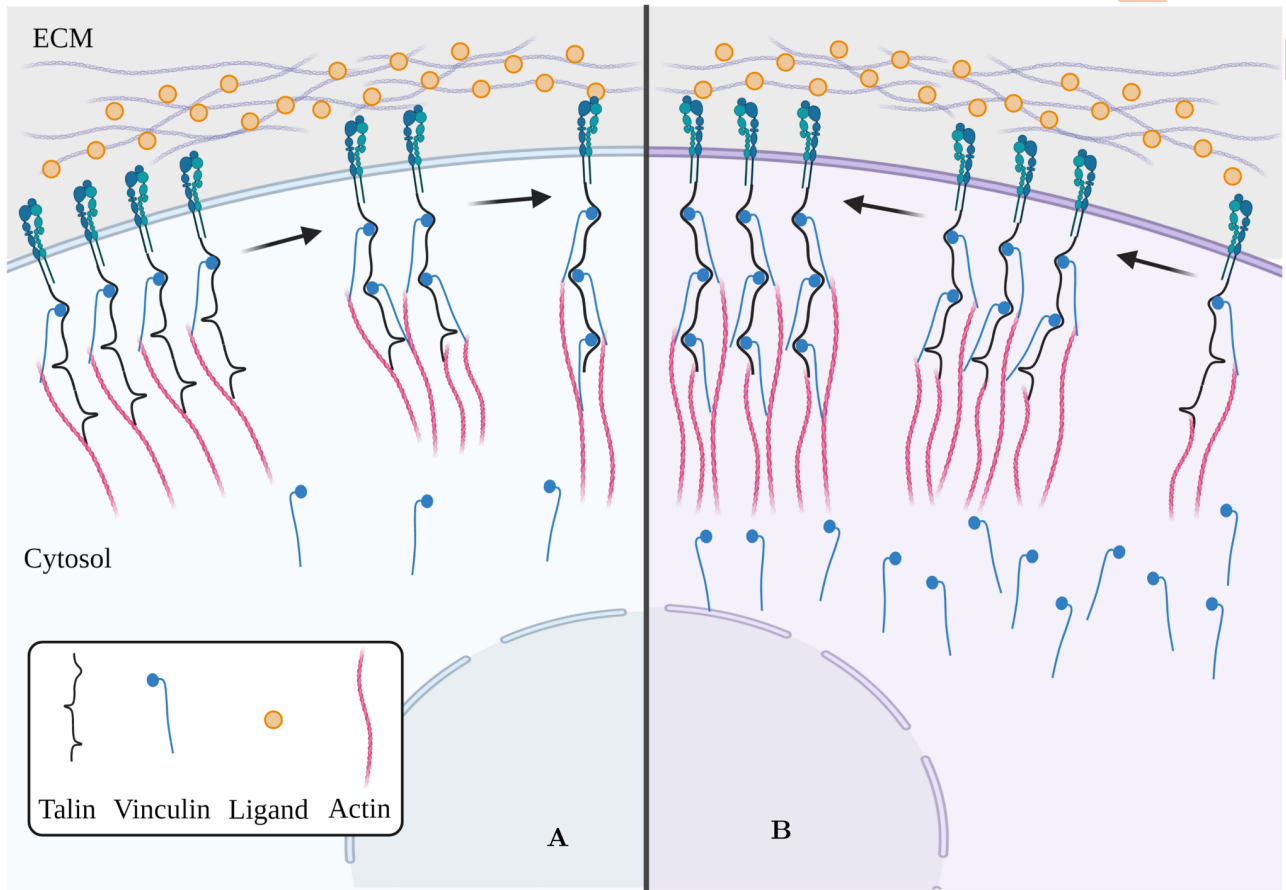
Fig 6. Vinculin concentration can influence maturation fraction. (A) and (B) are cell types or biological contexts where vinculin availability is low and high respectively. In A, the likelihood of vinculin binding to the exposed vinculin-binding sites on talin is low leading to a low maturation fraction. However, in B, due to a relatively higher vinculin availability, the integrin-actin link is highly likely to be reinforced by vinculin, increasing the maturation fraction. This figure was created using BioRender.com.

in the same trends of maturation across different stiffnesses but with slightly higher maturation fractions (Fig H in S1 Appendix).

An increase in v_u, the unloaded actin retrograde velocity, pushed the optimal substrate stiffness to softer substrates in line with previous computational studies [57, 60] and leads to lower MF (Fig 5). A higher retrograde velocity causes faster force build-up resulting in frictional slippage on softer substrates. Similar to k_{tal}, it also results in lower MF. On the contrary, increases in k_{act} pushed the optimal substrate stiffness towards stiffer substrates and increases MF (Fig 5), which is due to the 'strengthening' of clutches as they are more likely to bind actin, get stretched and recruit vinculin, and on average there are more AB clutches resulting in higher forces on softer substrates [57, 60].

Out of all the parameters, the stiffness of talin k_{tal}, initial vinculin concentration $initial_{vinc}$, talin refolding rate tal_{rf}, and the actin-binding rate k_{act} had the greatest influence on MF, similar for both an increase and decrease in the parameter values (Fig I in S1 Appendix). Importantly, the TDRM factor k_{sens}, and the cluster formation (k_{14f}, k_{15f} k_{16f}) and disassembly (k_{21f}, k_{22f}) rates had negligible influences on the MF and optimal stiffness (Figs I and J in S1 Appendix) for the tested range of values (±20%).

Discussion

Although cell-ECM adhesions are extensively studied, the effects of mechanical properties of the ECM and intracellular proteins on the early processes of adhesion assembly, maturation and traction force generation remain unclear. Here, we present a computational model that innovatively bridges the discrete mechanical and continuous biochemical aspects of adhesion formation. Our model captures key trends in the maturation fraction (MF) of NAs, actin retrograde velocity, and the periods of bond formation-rupture cycles, all in agreement with experimental evidence [4, 18, 59, 62]. The predicted optimal substrate stiffness [4] and stiffness sensitivity range [57, 61] also lie within experimentally determined ranges.

While the predicted mean actin retrograde velocity across the stiffness range tested is in agreement with an experimental study using embryonic chick forebrain neurons [4], the agreement with the study of Elosegui-Artola and colleagues (2014) [36] is limited to the softer regimes where the biphasic trend is also seen (compare yellow and blue lines in Fig 4A). This discrepancy arises from the way reinforcement of adhesions is modelled. In particular, reinforcement in that study is modelled as an increase in the integrin density that occurs if a clutch experiences a force ≥ 87 pN, leading to an increase in integrin–ECM binding events and a larger number of bound clutches. In a recent computational study where reinforcement is also modelled similarly, a biphasic behaviour is observed just as in our model but with the optimal stiffness being around 10 pN/nm [38]. In our model, while there is an increase in the cluster size of clutches and additional vinculin recruitment leading to larger force-carrying capacities, there is no change in the number of available integrins or the adhesion formation rates.

In this study, we assume relatively fast kinetics for the signal molecule to keep the NA assembly and disassembly phases in line with experimental data [17]. It is important to note that there may be considerable differences in experimental results based on the cell types used, resulting in different time scales. However, since the model is relatively insensitive to changes in $signal_{thresh}$ (Figs I and J in S1 Appendix), and consequently changes in t_{sig}, the overall behaviour of the model is unlikely to change drastically when these parameters are tuned to represent specific cell types or, for instance, signal molecule kinetics. Thus, the generic signal molecule in the model can potentially represent the level of unphosphorylated FAK or similar molecules whose change in (phosphorylation) state can set off signalling cascades leading to adhesion disassembly. Future work should aim to determine the underlying factors that induce and influence adhesion disassembly so that the generic signal molecule can be replaced with more accurate formulations and interactions. In particular, the identification of such concrete factors could help in determining the settings of $signal_{thresh}$.

Based on our results, the factors affecting the NA disassembly dynamics play a more important role than those affecting assembly dynamics. We applied TDRM, an innovative method to account for spontaneous bond-rupture events in NA formation in an ODE framework. TDRM was necessary to establish the optimal stiffness because in its absence, maturation is highest on soft substrates as forces on the clutches build up slowly, giving long durations for maturation reactions to occur. TDRM counters this by increasing the rate of clutch-actin bond rupture and hence prevents maturation. With the baseline value of the TDRM factor k_{sens}, the effect of TDRM on the bond-rupture rate is highest on soft substrates and negligible on stiffer substrates due to the short clutch lifetimes. Walcott et al. (2011) [63] predicted and experimentally verified that disassembly processes begin earlier for soft substrates, and this arises from the force- and strain-dependent bond formation and rupture probabilities. In addition, cyclic mechanical reinforcement (CMR) of integrin-ligand bonds strengthens them, increasing the lifetimes, implying that on soft substrates where force-loading is relatively slow and force remains low for longer durations, these bonds are less reinforced and are more likely to break [53]. In previous studies,

CMR has been modelled as an increase in bond-dissociation rates at low forces [35, 38]. TDRM can be considered as a method to coarsely account for these processes. However, while the outcomes of TDRM are similar to the effects of CMR as modelled in [35, 38], the differences between the two methods need to be investigated further. Surprisingly, the optimal stiffness was insensitive to changes in the parameter that controls the magnitude of TDRM (k_{sens}, (Fig 5B). This was unexpected since TDRM was essential for establishing an optimal stiffness implying a major role of this parameter in determining model behaviour (Figs F and G in S1 Appendix). It is likely that the explored sensitivity range (±20%) was too narrow to considerably change the behaviour of the model, which should be investigated more in-depth in the future. Note as well that in this study we performed a local sensitivity analysis focusing on those parameters that can directly be traced to a biological phenomenon (for instance k_{act}, $Initial_{vinc}$), those that we introduced as part of SDRM and TDRM (for instance k_{sens}, $signal_{thresh}$), or assumed (for instance, $tal_{rf_{factor}}$). Considering the non-linear nature of the model, it would be interesting in future studies, to conduct a more rigorous, global sensitivity analysis (i.e. using Bayesian Optimization) to further identify the most significant parameters of the model.

Another benefit of our model is that it allows the prediction of the maturation fraction of adhesions for a range of substrate stiffnesses. While there are no studies to the best of our knowledge that explicitly investigate the MFs for different substrate stiffnesses, the predicted range of MFs for the stiffness range tested in this study was within the range of experimentally determined fractions [18, 62].

Our sensitivity analysis results show that the MF is highly influenced by the concentration of integrins and vinculin available, the actin-binding rate, and the talin-refolding rate (Fig 5A). These factors can possibly be experimentally controlled, by introducing mutations in the proteins, allowing the predictions to be tested. Additionally, the MF and optimal stiffness were found to be insensitive to variations in the TDRM factor k_{sens} and the cluster formation and disassembly rates, suggesting that the model is locally robust to these factors and the parameters can be tuned to be specific to experimental conditions or cell lines. This suggests that the model can be used to predict the MFs for a variety of conditions by varying molecular stiffnesses, initial concentrations of talin, integrin, and vinculin, different clustering, maturation, and disassembly rates among many other parameters. This can potentially shed light on how traction force exerted by the cell is affected by biochemical alterations within the cell.

For instance, vinculin plays an important role in both cell-ECM adhesions and cell-cell adhesions through cadherins. Numerous studies indicate interdependence and cooperativity of these two processes, mediated through signal cascades or proteins that are essential in both types of adhesions, to varying degrees in different cell types [64–69]. While vinculin knockout studies have shown that traction force generation is impaired, with some studies reporting a decrease of nearly 50% in the absence of vinculin, overexpression of vinculin results in extremely strong adhesions that suppresses cell motility [70–75]. However, this leaves unanswered questions about how relatively less drastic changes in vinculin availability arising from cross-talk between integrins and cadherins adhesion complexes affect traction force generation and adhesion maturation. Our model predicts that a 20% decrease in the vinculin concentration results in a ∼9% increase in the actin retrograde velocity (or equivalently a 9% decrease in the traction force exerted due to lower MFs) at the optimal substrate stiffness (Fig 5). Thus, our model can be especially valuable to make predictions and generate hypotheses about how (local) adhesion protein concentrations influence the early processes of adhesion assembly, maturation, and traction force generation.

Overall, our model improves on previous studies in several aspects. Firstly, the process of maturation is more accurately captured by accounting for multiple vinculin recruitment events that

progressively increase the clutch stiffness in a continuous ODE framework. Previous studies either did not account for this or at most accounted for recruitment of one vinculin [4, 30–35]. Secondly, this model couples changes in discrete mechanical factors of adhesion maturation such as clutch stiffness with the continuous framework of biochemical reactions underlying adhesion maturation. This is particularly important because the continuous biochemical models do not explicitly account for force on the clutches, and discrete mechanical models of adhesion formation do not capture the resulting experimentally measurable biochemical changes that occur.

While it is clear from our results that the adhesion assembly and disassembly rates must be dynamic and dependent on a signal to achieve the maturation of only a fraction of the NAs that are initially formed, we acknowledge several limitations to this study. First, we do not model numerous proteins involved in the process of maturation or the continuous increase in the area of the adhesion [76]. Second, we simplified vinculin recruitment and growth of cluster size to occur in two discrete steps, and no spatial effects (e.g. proximity to an actin fibre, the distance of adhesion from the cell membrane) are accounted for. And third, we assume that integrins, talin and vinculin are available in roughly equal proportions near the adhesions (initial concentrations are the same), which may not necessarily be true. Despite these limitations, our model reproduced experimentally observed trends with respect to force, substrate stiffness, and time periods of oscillation in concentrations of the different seeds and clusts [4, 59, 60]. Furthermore, our results are reasonably close to discrete, stochastic computational studies as mentioned earlier even though our model bridges discrete and continuous aspects. The model thus provides a reliable foundation for further investigations.

What remains to be explored, perhaps by building on our model, is the interaction between the various signal cascades that regulate NA maturation. The ubiquitous signaling molecule FAK is also force-activated adding a further layer of interactions and complexity [77, 78]. In addition, the KANK family of proteins are known to impair the actin-binding capacity of talin, thereby weakening the integrin-actin linkage, and affecting the catch and slip bond dynamics [79]. They also play a role in targeting microtubules to focal adhesions which aids in their disassembly through multiple signal cascades [80]. By expanding the current model framework to include these interactions, it has the potential to robustly simulate the mechanochemical processes underlying mechanotransduction and provide valuable insight into cell signalling, communication and organization, hence contributing to advances in developmental biology and regenerative medicine.

Implementation

The model and the simulations were implemented using MATLAB R2020a [81]. All code and scripts used in this study are publicly available via GitHub at https://github.com/CarlierComputationalLab/force-dependent-adhesion-composition.git.

Supporting information

S1 Appendix. Detailed explanations of the methods (Text A), additional results (Text B), figures (Fig A—Fig N) and tables (Table A and Table B). [83–104] are cited in this file. (ZIP)

Acknowledgments

Author Contributions

Conceptualization: Kailas Shankar Honasoge, Zeynep Karagöz, Aurélie Carlier.

Data curation: Kailas Shankar Honasoge, Zeynep Karagöz.

Formal analysis: Kailas Shankar Honasoge, Zeynep Karagöz, Aurélie Carlier.

Funding acquisition: Aurélie Carlier.

Methodology: Kailas Shankar Honasoge, Zeynep Karagöz, Aurélie Carlier.

Supervision: Benjamin T. Goult, Haguy Wolfenson, Vanessa L. S. LaPointe, Aurélie Carlier.

Visualization: Kailas Shankar Honasoge, Zeynep Karagöz, Aurélie Carlier.

Writing – original draft: Kailas Shankar Honasoge, Zeynep Karagöz, Aurélie Carlier.

Writing – review & editing: Kailas Shankar Honasoge, Zeynep Karagöz, Benjamin T. Goult, Haguy Wolfenson, Vanessa L. S. LaPointe, Aurélie Carlier.

References

1. Thomas JW, Cooley MA, Broome JM, Salgia R, Griffin JD, Lombardo CR, et al. The Role of Focal Adhesion Kinase Binding in the Regulation of Tyrosine Phosphorylation of Paxillin *. Journal of Biological Chemistry. 1999; 274:36684–36692. https://doi.org/10.1074/jbc.274.51.36684 PMID: 10593973

2. Hynes RO. Integrins: A family of cell surface receptors. Cell. 1987; 48:549–554. https://doi.org/10.1016/0092-8674(87)90233-9 PMID: 3028640

3. Campbell ID, Humphries MJ. Integrin Structure, Activation, and Interactions. Cold Spring Harbor Perspectives in Biology. 2011; 3:a004994. https://doi.org/10.1101/cshperspect.a004994 PMID: 21421922

4. Chan CE, Odde DJ. Traction dynamics of filopodia on compliant substrates. Science (New York, NY). 2008; 322:1687–1691. https://doi.org/10.1126/science.1163595 PMID: 19074349

5. Jiang G, Giannone G, Critchley DR, Fukumoto E, Sheet MP. Two-piconewton slip bond between fibronectin and the cytoskeleton depends on talin. Nature. 2003; 424:334–337. https://doi.org/10.1038/nature01805 PMID: 12867986

6. Berrier AL, Yamada KM. Cell–matrix adhesion. Journal of Cellular Physiology. 2007; 213:565–573. https://doi.org/10.1002/jcp.21237 PMID: 17680633

7. Horton ER, Byron A, Askari JA, Ng DHJ, Millon-Frémillon A, Robertson J, et al. Definition of a consensus integrin adhesome and its dynamics during adhesion complex assembly and disassembly. Nature Cell Biology 2015 17:12. 2015; 17:1577–1587. https://doi.org/10.1038/ncb3257 PMID: 26479319

8. Winograd-Katz SE, Fässler R, Geiger B, Legate KR. The integrin adhesome: from genes and proteins to human disease. Nature Reviews Molecular Cell Biology 2014 15:4. 2014; 15:273–288. https://doi.org/10.1038/nrm3769 PMID: 24651544

9. Fortunato IC, Sunyer R. The Forces behind Directed Cell Migration. Biophysica 2022, Vol 2, Pages 548-563. 2022; 2:548–563. https://doi.org/10.3390/biophysica2040046

10. Cluzel C, Saltel F, Lussi J, Paulhe F, Imhof BA, Wehrle-Haller B. The mechanisms and dynamics of $\alpha_V \beta 3$ integrin clustering in living cells. Journal of Cell Biology. 2005; 171:383–392. https://doi.org/10.1083/jcb.200503017 PMID: 16247034

11. Pinon P, Pärssinen J, Vazquez P, Bachmann M, Rahikainen R, Jacquier MC, et al. Talin-bound NPLY motif recruits integrin-signaling adapters to regulate cell spreading and mechanosensing. Journal of Cell Biology. 2014; 205:265–281. https://doi.org/10.1083/jcb.201308136 PMID: 24778313

12. Humphries JD, Wang P, Streuli C, Geiger B, Humphries MJ, Ballestrem C. Vinculin controls focal adhesion formation by direct interactions with talin and actin. The Journal of cell biology. 2007; 179:1043–1057. https://doi.org/10.1083/jcb.200703036 PMID: 18056416

13. Hynes RO. Integrins: Bidirectional, Allosteric Signaling Machines. Cell. 2002; 110:673–687. https://doi.org/10.1016/S0092-8674(02)00971-6 PMID: 12297042

14. Askari JA, Tynan CJ, Webb SED, Martin-Fernandez ML, Ballestrem C, Humphries MJ. Focal adhesions are sites of integrin extension. Journal of Cell Biology. 2010; 188:891–903. https://doi.org/10.1083/jcb.200907174 PMID: 20231384

15. Bachir AI, Zareno J, Moissoglu K, Plow EF, Gratton E, Horwitz AR. Integrin-Associated Complexes Form Hierarchically with Variable Stoichiometry in Nascent Adhesions. Current Biology. 2014; 24:1845–1853. https://doi.org/10.1016/j.cub.2014.07.011 PMID: 25088556

16. Changede R, Xu X, Margadant F, Sheetz MP. Nascent Integrin Adhesions Form on All Matrix Rigidities after Integrin Activation. Developmental cell. 2015; 35:614–621. https://doi.org/10.1016/j.devcel.2015.11.001 PMID: 26625956

17. Choi CK, Vicente-Manzanares M, Zareno J, Whitmore LA, Mogilner A, Horwitz AR. Actin and alpha-actinin orchestrate the assembly and maturation of nascent adhesions in a myosin II motor-independent manner. Nature cell biology. 2008; 10:1039–1050. https://doi.org/10.1038/ncb1763 PMID: 19160484

18. Han SJ, Azarova EV, Whitewood AJ, Bachir A, Guttierrez E, Groisman A, et al. Pre-complexation of talin and vinculin without tension is required for efficient nascent adhesion maturation. eLife. 2021; 10. https://doi.org/10.7554/eLife.66151 PMID: 33783351

19. Pelham RJ, Wang YL. Cell locomotion and focal adhesions are regulated by substrate flexibility. Proceedings of the National Academy of Sciences of the United States of America. 1997; 94:13661–13665. https://doi.org/10.1073/pnas.94.25.13661 PMID: 9391082

20. Schoenwaelder SM, Burridge K. Bidirectional signaling between the cytoskeleton and integrins. Current opinion in cell biology. 1999; 11:274–286. https://doi.org/10.1016/S0955-0674(99)80037-4 PMID: 10209151

21. Rothenberg KE, Scott DW, Christoforou N, Hoffman BD. Vinculin Force-Sensitive Dynamics at Focal Adhesions Enable Effective Directed Cell Migration. Biophysical Journal. 2018; 114:1680–1694. https://doi.org/10.1016/j.bpj.2018.02.019 PMID: 29642037

22. Zhou DW, Fernández-Yagüe MA, Holland EN, García AF, Castro NS, O'Neill EB, et al. Force-FAK signaling coupling at individual focal adhesions coordinates mechanosensing and microtissue repair. Nature Communications 2021 12:1. 2021; 12:1–13. https://doi.org/10.1038/s41467-021-22602-5 PMID: 33883558

23. Sun Z, Costell M, Fässler R. Integrin activation by talin, kindlin and mechanical forces. Nature Cell Biology 2019 21:1. 2019; 21:25–31. https://doi.org/10.1038/s41556-018-0234-9 PMID: 30602766

24. Yao M, Goult BT, Klapholz B, Hu X, Toseland CP, Guo Y, et al. The mechanical response of talin. Nature Communications 2016 7:1. 2016; 7:1–11. https://doi.org/10.1038/ncomms11966 PMID: 27384267

25. Goult BT, Yan J, Schwartz MA. Talin as a mechanosensitive signaling hub. The Journal of cell biology. 2018; 217:3776–3784. https://doi.org/10.1083/jcb.201808061 PMID: 30254032

26. Novikova EA, Storm C. Contractile Fibers and Catch-Bond Clusters: a Biological Force Sensor? Biophysical Journal. 2013; 105:1336–1345. https://doi.org/10.1016/j.bpj.2013.07.039 PMID: 24047984

27. Aratyn-Schaus Y, Gardel ML. Transient Frictional Slip between Integrin and the ECM in Focal Adhesions under Myosin II Tension. Current Biology. 2010; 20:1145–1153. https://doi.org/10.1016/j.cub.2010.05.049 PMID: 20541412

28. Giannone G, Dubin-Thaler BJ, Rossier O, Cai Y, Chaga O, Jiang G, et al. Lamellipodial actin mechanically links myosin activity with adhesion site formation. Cell. 2007; 128:561. https://doi.org/10.1016/j.cell.2006.12.039 PMID: 17289574

29. Goult BT, von Essen M, Hytönen VP. The mechanical cell—the role of force dependencies in synchronising protein interaction networks. Journal of Cell Science. 2022; 135. https://doi.org/10.1242/jcs.259769 PMID: 36398718

30. Sonn-Segev A, Bernheim-Groswasser A, Roichman Y, Schmitz S, Smith-Palmer J, Sakamoto T, et al. Model for adhesion clutch explains biphasic relationship between actin flow and traction at the cell leading edge. Physical Biology. 2015; 12:035002. https://doi.org/10.1088/1478-3975/12/3/035002

31. Macdonald A, Horwitz AR, Lauffenburger DA. Kinetic model for lamellipodal actin-integrin 'clutch' dynamics. Cell adhesion & migration. 2008; 2:95–105. https://doi.org/10.4161/cam.2.2.6210 PMID: 19262096

32. Lai T, Chiam KH. Mechanochemical model of cell migration on substrates of varying stiffness. Physical Review E—Statistical, Nonlinear, and Soft Matter Physics. 2011; 84:061907. https://doi.org/10.1103/PhysRevE.84.061907 PMID: 22304116

33. Cirit M, Krajcovic M, Choi CK, Welf ES, Horwitz AF, Haugh JM. Stochastic Model of Integrin-Mediated Signaling and Adhesion Dynamics at the Leading Edges of Migrating Cells. PLOS Computational Biology. 2010; 6:e1000688. https://doi.org/10.1371/journal.pcbi.1000688 PMID: 20195494

34. Cheng B, Lin M, Li Y, Huang G, Yang H, Genin GM, et al. An Integrated Stochastic Model of Matrix-Stiffness-Dependent Filopodial Dynamics. Biophysical Journal. 2016; 111:2051. https://doi.org/10.1016/j.bpj.2016.09.026 PMID: 27806285

35. Elosegui-Artola A, Oria R, Chen Y, Kosmalska A, Pérez-González C, Castro N, et al. Mechanical regulation of a molecular clutch defines force transmission and transduction in response to matrix rigidity. Nature Cell Biology 2016 18:5. 2016; 18:540–548. https://doi.org/10.1038/ncb3336 PMID: 27065098

36. Elosegui-Artola A, Bazellières E, Allen MD, Andreu I, Oria R, Sunyer R, et al. Rigidity sensing and adaptation through regulation of integrin types. Nature materials. 2014; 13:631. https://doi.org/10.1038/nmat3960 PMID: 24793358

37. Tan SJ, Chang AC, Anderson SM, Miller CM, Prahl LS, Odde DJ, et al. Regulation and dynamics of force transmission at individual cell-matrix adhesion bonds. Science Advances. 2020; 6. https://doi.org/10.1126/sciadv.aax0317 PMID: 32440534

38. Venturini C, Sáez P. A multi-scale clutch model for adhesion complex mechanics. bioRxiv. 2023; p. 2023.01.09.523273. https://doi.org/10.1371/journal.pcbi.1011250 PMID: 37450544

39. Yao M, Goult BT, Chen H, Cong P, Sheetz MP, Yan J. Mechanical activation of vinculin binding to talin locks talin in an unfolded conformation. Scientific Reports 2014 4:1. 2014; 4:1–7. https://doi.org/10.1038/srep04610

40. Webb DJ, Donais K, Whitmore LA, Thomas SM, Turner CE, Parsons JT, et al. FAK–Src signalling through paxillin, ERK and MLCK regulates adhesion disassembly. Nature Cell Biology 2004 6:2. 2004; 6:154–161. PMID: 14743221

41. Kong F, García AJ, Mould AP, Humphries MJ, Zhu C. Demonstration of catch bonds between an integrin and its ligand. Journal of Cell Biology. 2009; 185:1275–1284. https://doi.org/10.1083/jcb.200810002 PMID: 19564406

42. Rio AD, Perez-Jimenez R, Liu R, Roca-Cusachs P, Fernandez JM, Sheetz MP. Stretching single talin rod molecules activates vinculin binding. Science. 2009; 323:638–641. https://doi.org/10.1126/science.1162912 PMID: 19179532

43. Gingras AR, Ziegler WH, Frank R, Barsukov IL, Roberts GCK, Critchley DR, et al. Mapping and Consensus Sequence Identification for Multiple Vinculin Binding Sites within the Talin Rod. Journal of Biological Chemistry. 2005; 280:37217–37224. https://doi.org/10.1074/jbc.M508060200 PMID: 16135522

44. Bell GI. Models for the Specific Adhesion of Cells to Cells. Science. 1978; 200:618–627. https://doi.org/10.1126/science.347575 PMID: 347575

45. Wang Y, Yan J, Goult BT. Force-Dependent Binding Constants. Biochemistry. 2019; 58:4696–4709. https://doi.org/10.1021/acs.biochem.9b00453 PMID: 31315399

46. Stumpf BH, Ambriović-Ristov A, Radenovic A, Smith AS. Recent Advances and Prospects in the Research of Nascent Adhesions. Frontiers in Physiology. 2020; 11:1562.

47. Changede R, Sheetz M. Integrin and cadherin clusters: A robust way to organize adhesions for cell mechanics. BioEssays. 2017; 39:1–12. https://doi.org/10.1002/bies.201600123 PMID: 27930828

48. Oser M, Condeelis J. The Cofilin Activity Cycle in Lamellipodia and Invadopodia. Journal of cellular biochemistry. 2009; 108:1252. https://doi.org/10.1002/jcb.22372 PMID: 19862699

49. Hamadi A, Bouali M, Dontenwill M, Stoeckel H, Takeda K, Rondé P. Regulation of focal adhesion dynamics and disassembly by phosphorylation of FAK at tyrosine 397. Journal of cell science. 2005; 118:4415–4425. https://doi.org/10.1242/jcs.02565 PMID: 16159962

50. Vicente-Manzanares M, Horwitz AR. Adhesion dynamics at a glance. Journal of Cell Science. 2011; 124:3923. https://doi.org/10.1242/jcs.095653 PMID: 22194302

51. Lin K, Asaro RJ. Nascent Adhesion Clustering: Integrin-Integrin and Integrin-Substrate Interactions. Biophysica 2022, Vol 2, Pages 34-58. 2022; 2:34–58. https://doi.org/10.3390/biophysica2010004

52. Rashmi More SK, Wang Q, Vomhof-DeKrey EE, Porter JE, Basson MD. ZINC40099027 activates human focal adhesion kinase by accelerating the enzymatic activity of the FAK kinase domain. Pharmacology Research & Perspectives. 2021; 9(2):e00737. https://doi.org/10.1002/prp2.737 PMID: 33715263

53. Kong F, Li Z, Parks WM, Dumbauld DW, García AJ, Mould AP, et al. Cyclic mechanical reinforcement of integrin-ligand interactions. Molecular Cell. 2013; 49:1060–1068. https://doi.org/10.1016/j.molcel.2013.01.015 PMID: 23416109

54. Wang Y, Yao M, Baker KB, Gough RE, Le S, Goult BT, et al. Force-Dependent Interactions between Talin and Full-Length Vinculin. Journal of the American Chemical Society. 2021; 143:14726–14737. https://doi.org/10.1021/jacs.1c06223 PMID: 34463480

55. Bingcheng Yi, Qi Xu, Wei Liu An overview of substrate stiffness guided cellular response and its applications in tissue regeneration. Bioactive Materials. 2022.

56. Zhou DW, Lee TT, Weng S, Fu J, García AJ. Effects of substrate stiffness and actomyosin contractility on coupling between force transmission and vinculin–paxillin recruitment at single focal adhesions. Molecular Biology of the Cell. 2017; 28:1901. https://doi.org/10.1091/mbc.E17-02-0116 PMID: 28468976

57. Bangasser BL, Shamsan GA, Chan CE, Opoku KN, Tüzel E, Schlichtmann BW, et al. Shifting the optimal stiffness for cell migration. Nature Communications 2017 8:1. 2017; 8:1–10. https://doi.org/10.1038/ncomms15313 PMID: 28530245

58. Bangasser BL, Odde DJ. Master equation-based analysis of a motor-clutch model for cell traction force. Cellular and molecular bioengineering. 2013; 6:449. https://doi.org/10.1007/s12195-013-0296-5 PMID: 24465279

59. Gong Z, Szczesny SE, Caliari SR, Charrier EE, Chaudhuri O, Cao X, et al. Matching material and cellular timescales maximizes cell spreading on viscoelastic substrates. Proceedings of the National Academy of Sciences of the United States of America. 2018; 115:E2686–E2695. https://doi.org/10.1073/pnas.1716620115 PMID: 29507238

60. Bangasser BL, Rosenfeld SS, Odde DJ. Determinants of Maximal Force Transmission in a Motor-Clutch Model of Cell Traction in a Compliant Microenvironment. Biophysical Journal. 2013; 105:581. https://doi.org/10.1016/j.bpj.2013.06.027 PMID: 23931306

61. Selig M, Lauer JC, Hart ML, Rolauffs B. Mechanotransduction and Stiffness-Sensing: Mechanisms and Opportunities to Control Multiple Molecular Aspects of Cell Phenotype as a Design Cornerstone of Cell-Instructive Biomaterials for Articular Cartilage Repair. International Journal of Molecular Sciences 2020, Vol 21, Page 5399. 2020; 21:5399. https://doi.org/10.3390/ijms21155399 PMID: 32751354

62. Swaminathan V, Fischer RS, Waterman CM. The FAK-Arp2/3 interaction promotes leading edge advance and haptosensing by coupling nascent adhesions to lamellipodia actin. Molecular Biology of the Cell. 2016; 27:1085–1100. https://doi.org/10.1091/mbc.E15-08-0590 PMID: 26842895

63. Walcott S, Kim DH, Wirz D, Sun SX. Nucleation and Decay Initiation Are the Stiffness-Sensitive Phases of Focal Adhesion Maturation. Biophysical Journal. 2011; 101:2919–2928. https://doi.org/10.1016/j.bpj.2011.11.010 PMID: 22208190

64. Tsai J, Kam L. Rigidity-Dependent Cross Talk between Integrin and Cadherin Signaling. Biophysical Journal. 2009; 96:L39. https://doi.org/10.1016/j.bpj.2009.01.005 PMID: 19289031

65. Chen X, Gumbiner BM. Crosstalk between different adhesion molecules. Current opinion in cell biology. 2006; 18:572–578. https://doi.org/10.1016/j.ceb.2006.07.002 PMID: 16859906

66. McCain ML, Lee H, Aratyn-Schaus Y, Kléber AG, Parker KK. Cooperative coupling of cell-matrix and cell-cell adhesions in cardiac muscle. Proceedings of the National Academy of Sciences of the United States of America. 2012; 109:9881–9886. https://doi.org/10.1073/pnas.1203007109 PMID: 22675119

67. Bays JL, DeMali KA. Vinculin in cell–cell and cell–matrix adhesions. Cellular and Molecular Life Sciences 2017 74:16. 2017; 74:2999–3009. https://doi.org/10.1007/s00018-017-2511-3 PMID: 28401269

68. Mertz AF, Che Y, Banerjee S, Goldstein JM, Rosowski KA, Revilla SF, et al. Cadherin-based intercellular adhesions organize epithelial cell-matrix traction forces. Proceedings of the National Academy of Sciences of the United States of America. 2013; 110:842–847. https://doi.org/10.1073/pnas.1217279110 PMID: 23277553

69. Rooij JD, Kerstens A, Danuser G, Schwartz MA, Waterman-Storer CM. Integrin-dependent actomyosin contraction regulates epithelial cell scattering. The Journal of Cell Biology. 2005; 171:153. https://doi.org/10.1083/jcb.200506152 PMID: 16216928

70. Rahman A, Carey SP, Kraning-Rush CM, Goldblatt ZE, Bordeleau F, Lampi MC, et al. Vinculin regulates directionality and cell polarity in two- and three-dimensional matrix and three-dimensional microtrack migration. Molecular Biology of the Cell. 2016; 27:1431. https://doi.org/10.1091/mbc.E15-06-0432 PMID: 26960796

71. Thievessen I, Thompson PM, Berlemont S, Plevock KM, Plotnikov SV, Zemljic-Harpf A, et al. Vinculin-actin interaction couples actin retrograde flow to focal adhesions, but is dispensable for focal adhesion growth. Journal of Cell Biology. 2013; 202:163–177. https://doi.org/10.1083/jcb.201303129 PMID: 23836933

72. Dumbauld DW, Lee TT, Singh A, Scrimgeour J, Gersbach CA, Zamir EA, et al. How vinculin regulates force transmission. Proceedings of the National Academy of Sciences of the United States of America. 2013; 110:9788–9793. https://doi.org/10.1073/pnas.1216209110 PMID: 23716647

73. Mierke CT, Kollmannsberger P, Zitterbart DP, Smith J, Fabry B, Goldmann WH. Mechano-coupling and regulation of contractility by the vinculin tail domain. Biophysical journal. 2008; 94:661–670. https://doi.org/10.1529/biophysj.107.108472 PMID: 17890382

74. Fernandez JLR, Geiger B, Salomon D, Ben-Ze'ev A. Suppression of vinculin expression by antisense transfection confers changes in cell morphology, motility, and anchorage-dependent growth of 3T3 cells. The Journal of Cell Biology. 1993; 122:1285. https://doi.org/10.1083/jcb.122.6.1285

75. Fernández JLR, Geiger B, Salomon D, Ben-Ze'ev A. Overexpression of vinculin suppresses cell motility in BALB/c 3T3 cells. Cell motility and the cytoskeleton. 1992; 22:127–134. https://doi.org/10.1002/cm.970220206

76. Geiger B, Yamada KM. Molecular Architecture and Function of Matrix Adhesions. Cold Spring Harbor Perspectives in Biology. 2011; 3:a005033. https://doi.org/10.1101/cshperspect.a005033 PMID: 21441590

77. Domingos PP, Fonseca PM, Nadruz W, Franchini KG. Load-induced focal adhesion kinase activation in the myocardium: Role of stretch and contractile activity. American Journal of Physiology—Heart and Circulatory Physiology. 2002; 282. PMID: 11788403

78. Tomar A, Schlaepfer DD. Focal adhesion kinase: switching between GAPs and GEFs in the regulation of cell motility. Current Opinion in Cell Biology. 2009; 21:676–683. https://doi.org/10.1016/j.ceb.2009.05.006 PMID: 19525103

79. Sun Z, Tseng HY, Tan S, Senger F, Kurzawa L, Dedden D, et al. Kank2 activates talin, reduces force transduction across integrins and induces central adhesion formation. Nature Cell Biology 2016 18:9. 2016; 18:941–953.

80. Bouchet BP, Gough RE, Ammon YC, van de Willige D, Post H, Jacquemet G, et al. Talin-KANK1 interaction controls the recruitment of cortical microtubule stabilizing complexes to focal adhesions. eLife. 2016; 5. https://doi.org/10.7554/eLife.18124 PMID: 27410476

81. Inc TM. MATLAB version: 9.13.0 (R2022b); 2022. Available from: https://www.mathworks.com.

82. Lansey JC. Beautiful and distinguishable line colors + colormap; 2023. Available from: https://www.mathworks.com/matlabcentral/fileexchange/42673-beautiful-and-distinguishable-line-colors-colormap.

83. Huang DL, Bax NA, Buckley CD, Weis WI, Dunn AR. Vinculin forms a directionally asymmetric catch bond with F-actin. Science (New York, NY). 2017; 357:703. https://doi.org/10.1126/science.aan2556 PMID: 28818948

84. Roca-Cusachs P, Iskratsch T, Sheetz MP. Finding the weakest link-exploring integrin-mediated mechanical molecular pathways. Journal of Cell Science. 2012; 125:3025–3038. https://doi.org/10.1242/jcs.095794 PMID: 22797926

85. Calderwood DA. Integrin activation. Journal of Cell Science. 2004; 117:657–666. https://doi.org/10.1242/jcs.01014 PMID: 14754902

86. Li J, Springer TA. Energy landscape differences among integrins establish the framework for understanding activation. Journal of Cell Biology. 2018; 217:397–412. https://doi.org/10.1083/jcb.201701169 PMID: 29122968

87. Miller AE, Hu P, Barker TH. Feeling Things Out: Bidirectional Signaling of the Cell–ECM Interface, Implications in the Mechanobiology of Cell Spreading, Migration, Proliferation, and Differentiation. Advanced Healthcare Materials. 2020; 9:1901445. https://doi.org/10.1002/adhm.201901445 PMID: 32037719

88. Ellis SJ, Lostchuck E, Goult BT, Bouaouina M, Fairchild MJ, López-Ceballos P, et al. The Talin Head Domain Reinforces Integrin-Mediated Adhesion by Promoting Adhesion Complex Stability and Clustering. PLoS Genetics. 2014; 10. https://doi.org/10.1371/journal.pgen.1004756 PMID: 25393120

89. Roca-Cusachs P, Gauthier NC, del Rio A, Sheetz MP. Clustering of $\alpha 5\beta 1$ integrins determines adhesion strength whereas $\alpha v\beta 3$ and talin enable mechanotransduction. Proceedings of the National Academy of Sciences of the United States of America. 2009; 106:16245–16250. https://doi.org/10.1073/pnas.0902818106 PMID: 19805288

90. Schvartzman M, Palma M, Sable J, Abramson J, Hu X, Sheetz MP, et al. Nanolithographic control of the spatial organization of cellular adhesion receptors at the single-molecule level. Nano Letters. 2011; 11:1306–1312. https://doi.org/10.1021/nl104378f PMID: 21319842

91. Cooper G. The Cell: A Molecular Approach. 2nd edition. Sinauer Associates; 2000.

92. Molloy JE, Burns JE, Kendrick-Jones B, Tregear RT, White DCS. Movement and force produced by a single myosin head. Nature 1995 378:6553. 1995; 378:209–212. PMID: 7477328

93. Kee YS, Robinson DN. Motor Proteins: Myosin Mechanosensors. Current Biology. 2008; 18:R860–R862. https://doi.org/10.1016/j.cub.2008.07.071 PMID: 18812080

94. Franz CM, Müller DJ. Analyzing focal adhesion structure by atomic force microscopy. Journal of Cell Science. 2005; 118:5315–5323. https://doi.org/10.1242/jcs.02653 PMID: 16263758

95. Vicente-Manzanares M, Zareno J, Whitmore L, Choi C, Horwitz AF. Regulation of protrusion, adhesion dynamics, and polarity by myosins IIA and IIB in migrating cells. Journal of Cell Biology. 2007; 176:573–580. https://doi.org/10.1083/jcb.200612043 PMID: 17312025

96. Okeyo KO, Adachi T, Hojo M. Dynamic coupling between actin network flow and turnover revealed by flow mapping in the lamella of crawling fragments. Biochemical and Biophysical Research Communications. 2009; 390:797–802. https://doi.org/10.1016/j.bbrc.2009.10.052 PMID: 19836353

97. Franco SJ, Rodgers MA, Perrin BJ, Han J, Bennin DA, Critchley DR, et al. Calpain-mediated proteolysis of talin regulates adhesion dynamics. Nature Cell Biology 2004 6:10. 2004; 6:977–983. https://doi.org/10.1038/ncb1175 PMID: 15448700

98. Bhatt A, Kaverina I, Otey C, Huttenlocher A. Regulation of focal complex composition and disassembly by the calcium-dependent protease calpain. Journal of Cell Science. 2002; 115:3415–3425. https://doi.org/10.1242/jcs.115.17.3415 PMID: 12154072

99. Dembo M, Torney DC, Saxman K, Hammer D. The reaction-limited kinetics of membrane-to-surface adhesion and detachment. Proceedings of the Royal Society B: Biological Sciences. 1988; 234:55–83. PMID: 2901109

100. Choi YI, Duke-Cohan JS, Chen W, Liu B, Rossy J, Tabarin T, et al. Dynamic control of β1 integrin adhesion by the plexinD1-sema3E axis. Proceedings of the National Academy of Sciences of the United States of America. 2014; 111:379–384. https://doi.org/10.1073/pnas.1314209111 PMID: 24344262

101. Chen W, Lou J, Zhu C. Forcing Switch from Short- to Intermediate- and Long-lived States of the αA Domain Generates LFA-1/ICAM-1 Catch Bonds. Journal of Biological Chemistry. 2010; 285:35967–35978. https://doi.org/10.1074/jbc.M110.155770 PMID: 20819952

102. Owen LM, Bax NA, Weis WI, Dunn AR. The C-terminal actin-binding domain of talin forms an asymmetric catch bond with F-actin. Proceedings of the National Academy of Sciences of the United States of America. 2022; 119. https://doi.org/10.1073/pnas.2109329119 PMID: 35245171

103. Lavelin I, Wolfenson H, Patla I, Henis YI, Medalia O, Volberg T, et al. Differential Effect of Actomyosin Relaxation on the Dynamic Properties of Focal Adhesion Proteins. PLOS ONE. 2013; 8:e73549. https://doi.org/10.1371/journal.pone.0073549 PMID: 24039980

104. Cheng B, Wan W, Huang G, Li Y, Genin GM, Mofrad MRK, et al. Nanoscale integrin cluster dynamics controls cellular mechanosensing via FAKY397 phosphorylation. Science Advances. 2020; 6. https://doi.org/10.1126/sciadv.aax1909 PMID: 32181337